Reply to reviewer #1

Comment 1: Line 138: The authors should clarify the information on which instrument dataset was used for each data product. Were the moments shown in Figure 2c-2e recalculated from the FPI distribution functions? Or are they the default moments calculated over the full FPI energy range?

Response: Thanks for the referee's kind advice. We should have clarified the dataset information in Figure 2 on which instrument was used. So I added detailed information about dataset what we used to the description of Figure 2. The plasma moments (e.g. Ion parallel and perpendicular temperatures, ion, and electron densities and ion velocity) from FPI shown in Figure 2c-2e are all from MMS L2 data products. They are default moments calculated over the full FPI energy range from 10 eV to 30 keV. But the O^+ density shown in Figure 2f is recalculated from HPCA distribution functions at energies from 1 to 40 keV. From the O^+ fluxes shown in Figure 2j, there still exists a large number of fluxes below 1 keV in the magnetosheath. This part of O^+ fluxes is fake and contamination from high proton fluxes. So we consider the number density of O^+ at energies from 1 to 40 keV is more appropriate to represent the true O^+ in the magnetopause. While the H^+ density (over the full HPCA energy range) from L2 data products are used in Figure 2f. The magnetic and electric fields in GSM are from FGM and EDP, respectively. The last four panels of Figure 2 show the omnidirectional differential fluxes of four individual ion species, H^+, O^+, He^+ and He^{++} measured by HPCA, respectively. See Line 198-207 in "Tracked change" manuscript.

Comment 2: Line 140 (Figure 2f): The calculations performed to derive the >1 keV O^+ density need to be described to inform the reader how the HPCA energy ranges were specified for those calculations. If a software package was used, then details of the software package and a citation to it should be included. The >1keV H^+ density could also be plotted in this figure panel.

Response: Thanks for the referee's good suggestion. As mentioned before, the >1 keV O^+ density (shown in Figure 2f) recalculated from the HPCA distribution functions at energies from 1 to 40 keV. As your suggestion, I also plotted the H^+ density over the full FPI energy range from 10 eV to 40 keV in Figure 2f for better comparison. Because of H^+ measurements from HPCA is accurate and the H^+ mean energy in the magnetosheath is typically 0.3 keV, so we used the H^+ density (over the full HPCA energy range) from L2 data products. These O^+ density calculations are used The Space Physics Environment Data Analysis System (SPEDAS) software package. More details about SPEDAS can be found in Angelopoulos et al. (2019) and cited as (Angelopoulos, V., Cruce, P., Drozdov, A. et al. Space Sci Rev (2019) 215: 9. https://doi.org/10.1007/s11214-018-0576-4). We also cited this paper in our revised manuscript, see Line 144-148 and Figure 2f in "Tracked change" manuscript.
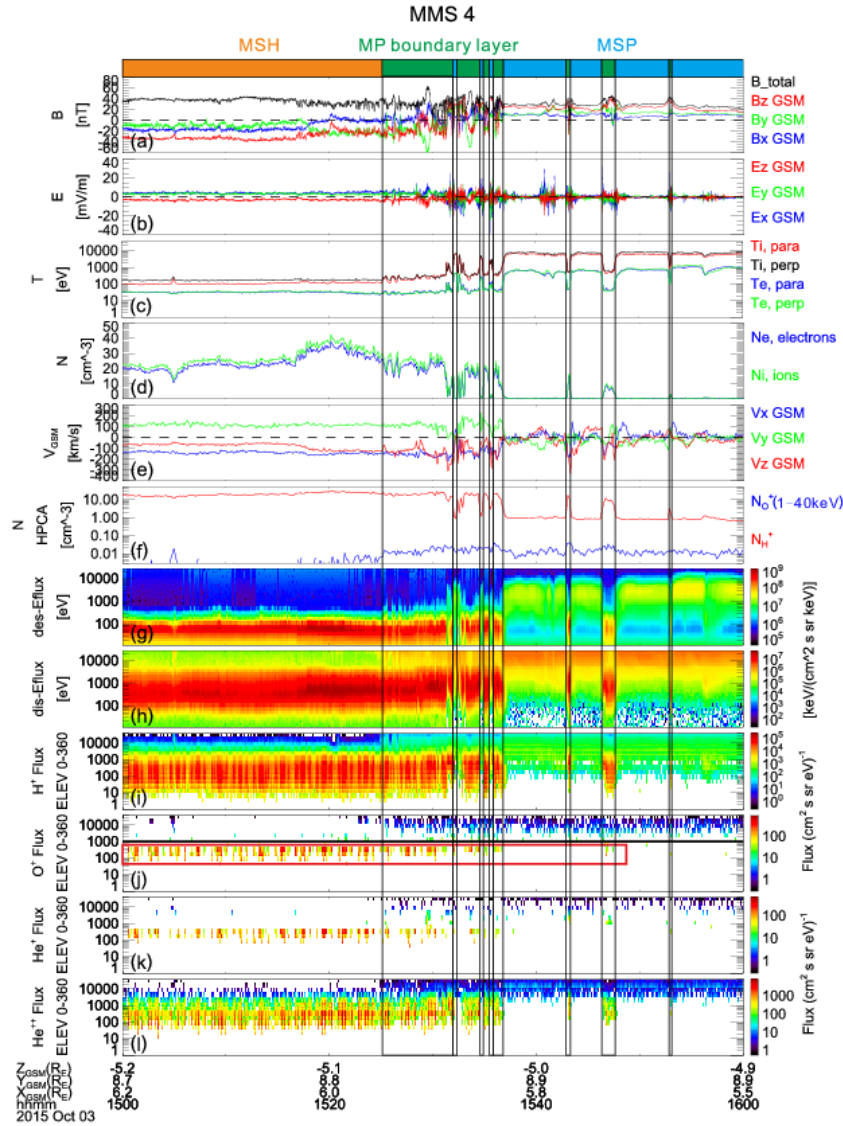
Figure 2. The energetic O⁺ are observed at the magnetopause during an intense substorm on 03 October 2015 by MMS 4. From top to bottom are (a) the magnetic field three components, Bx (blue line), By (gree line), Bz (red line) and the total magnitude Bt (black line), (b) the electric field three components, Ex (blue), Ey (gree) and Ez (red), (c) Ion parallel (red) and perpendicular(black) temperatures, (d) The number density of ion (green) and electron (blue), (e) three components of the ion velocity, (f) number density of H⁺ (over the full HPCA energy range) and O⁺ (at energies from 1 to 40 keV), (g) electron omnidirectional differential energy fluxes, (h) ion omnidirectional differential energy fluxes, (i) to (l) present omnidirectional differential particle fluxes of H⁺, O⁺, He⁺, and He⁺⁺, respectively. The Geocentric Solar Magnetospheric (GSM) coordinate system is adopted. The thick bars at the top of the panel represent different regions encountered on this magnetopause crossing event. The orange and blue bars represent the magnetosheath and the magnetosphere, respectively. The green bar represents the magnetopause boundary layer. The black horizontal line in figure 2j is at 1 keV and the O⁺ contamination from high H⁺ fluxes is indicated by the red box. The FPI data in Figure 2c-e and 2g-h are from FPI L2 data product and in the fast mode.

Comment 3: Line 158-164: The magnetopause identification criteria are not very convincing. Recommend carefully defining these criteria, as all statistics are derived based on the magnetopause identification. Recommend the authors review identification criteria used in previous works. For example, Haaland et al. (2016) and (2019) describe magnetopause observations by Cluster and THEMIS: Haaland, S., Reistad, J., Tenfjord, P., Gjerloev, J., Maes, L., DeKeyser, J., Maggiolo,R., Anekallu, C., and Dorville, N. (2014), Characteristics of the flank magnetopause:Cluster observations, J. Geophys. Res. Space Physics, 119, 9019–9037,doi:10.1002/2014JA020539.

Haaland, S., Runov, A., Artemyev, A., & Angelopoulos, V. (2019). Characteristics of the flank magnetopause: THEMIS observations. Journal of Geophysical Research: Space Physics, 124, 3421–3435. https://doi.org/10.1029/2019JA026459. Paschmann et al. (2018) describe magnetopause identification and observations by MMS:

Paschmann, G., Haaland, S. E., Phan, T. D., Sonnerup, B. U. Ö., Burch, J. L., Torbert, R. B., et al. (2018). Large-scale survey of the structure of the dayside magnetopause by MMS. Journal of Geophysical Research: Space Physics, 123, 2018–2033. https://doi.org/10.1002/2017JA025121.

Response: Thanks for the referee's kind suggestion and well recommend. We read the papers your recommended and found they did detailed work for magnetopause identification. It deepens my understanding of the flank magnetopause characteristics and helps me identifying the magnetopause more convincing. In this study, we mainly focus on the O^+ in the dusk flank magnetopause boundary layer. According to the magnetic field, B is about 40 nT and O^+ temperature, T is about 10 keV in this study, we can draw the O^+ gyroradius is about 1020 km. From Haaland et al. (2014), the flank magnetopause thickness varies from 150 to 5000 km with a median thickness of around 1150 at dusk. Thus the gyroradius of ten keV O^+ is comparable to magnetopause thickness. In that situation, O^+ will show the finite Larmor radius effects and the MMS detect partial gyro motion in the magnetopause. For acquiring complete O^+ distribution functions, we need to measure O^+ in more large spatial scales. So in this study, we focus on the magnetopause boundary layer judgment. The magnetopause boundary layers are identified here primarily through plasma fluxes and moments. The low-latitude boundary layer (LLBL) on the magnetospheric side of the magnetopause current layer and the magnetosheath boundary layer (MSBL) on the magnetosheath side of the magnetopause current layer can have densities and temperatures between that of the magnetosphere and magnetosheath. Ion jets are also signatures of passing through the magnetopause boundary layers. In this study, the separatrix between the magnetosheath and the magnetopause boundary layer is determined by the appearance of the magnetospheric electron. Similarily, the separatrix of the magnetosphere and the magnetopause boundary layer is determined by the magnetosheath electron disappearance. The revised details can be found in Line 221-233 in "Tracked change" manuscript.

Comment 4: Line 180: More details are needed to describe how the mean values of the H^+ and O^+ fluxes and densities were calculated.

Response: Thanks for the referee's kind advice. First, we determine the time interval of the magnetopause boundary layer crossings in each event. For example, on 03 October 2015 event, MMS 4 traversed the duskside magnetopause boundary layer from 15:25:10 to 15:36:50 UT judged by the typical characteristics in this region as mentioned before. Then, the H^+ and O^+ fluxes and densities were average during this time interval. We also give the error bars indicating 90% confidence intervals. We think these mean values represent the H^+ and O^+ fluxes and densities in the magnetopause boundary layer. See Line 232-233 in "Tracked change" manuscript.

Comment 5: Line 184: A more detailed description of how the substorm phase (i.e. expansion phase or recovery phase) was defined based on AE index is needed. The authors should use Figure 1 AE index to aid in their description.

Response: Thanks for the referee's suggestion. We should give more details to clarify how we define the substorm phase according to substorm indices, such as AU, AL, and AE index. First, we determined the time interval of the magnetopause boundary layer crossings in each event. Then, see how the substorm indices vary during that interval from the OMNI data. As Figure 1 shown, the time interval of the magnetopause boundary layer crossing is marked by the two blue dashed lines. As we know, the AE index is defined as AE=AU-AL. Generally, the substorm onset time is characteristic by the AL index starts to significantly decrease and the AE index significantly increase. During the substorm expansion phase, the AL index will decrease significantly. The interval of the AL index decrease from onset to its minimum is defined as the substorm expansion phase. Then it starts to increase and the interval of the AL index increase from the minimum to the quiet time level is regarded as the substorm recovery phase. In our event, the MMS4 crossed the magnetopause boundary layer from 15:25:10 to 15:36:50 UT on 3 October 2015. From Figure 1f, the AL index reached its minimum ~-750 nT and AE index reach the peak ~1000 nT at about 15:20 UT, then it started to increase to ~ -200 nT at the rest time of interest. The two blue dashed lines indicate the time interval of the magnetopause boundary layer crossing. According to the variation and peak value of the AU, AL and AE index in Figure 1e to 1g. The magnetopause boundary layer crossing occurred during the recovery phase of this intense substorm. The revised details can be found in Line 166-180 in "Tracked change" manuscript.
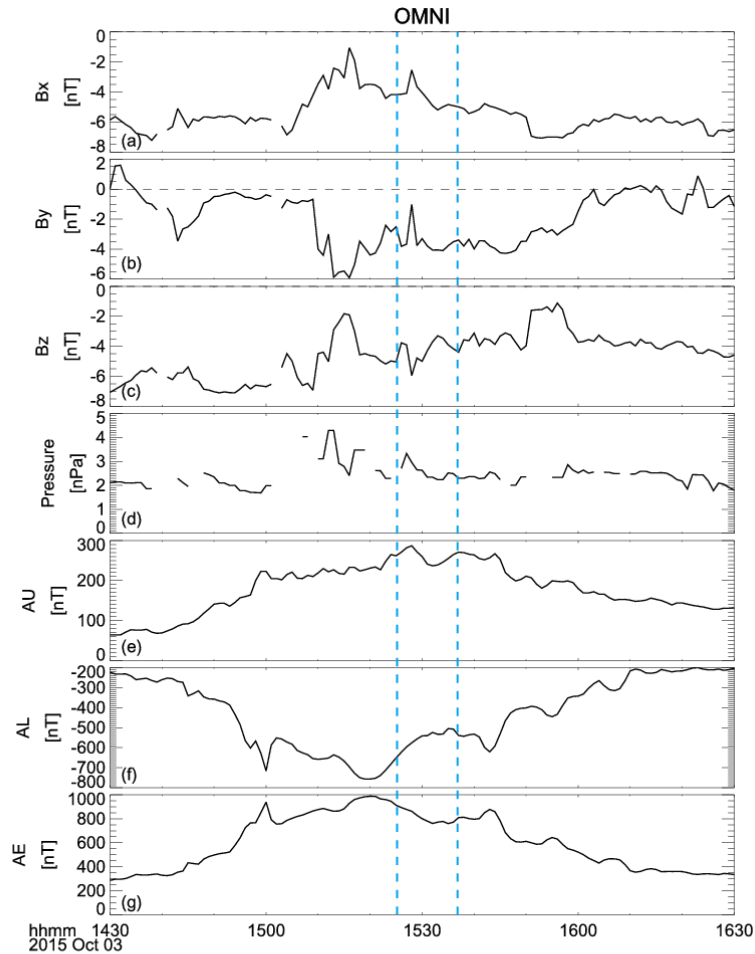
Figure 1. The three components IMF Bx, By, Bz, solar wind dynamic pressure, as well as AU, AL, and AE index from CDAweb OMNI data.

Comments 6: Line 202-209: Several narrow energy ranges used for comparing the O^+/H^+ density ratio are noted. It is important to describe for the reader how these energy ranges were used in the density ratio calculations. In addition, a description of why these energy ranges were chosen should be included. Did the authors consider calculating the density ratio for all energies >1 keV instead of calculating the ratios over individual energy ranges? A comparison of density ratios using both methods may be helpful to decide which method to use. Such procedural information on which analysis methodology was chosen could be included in an appendix.

Response: Thanks for carefully evaluating this manuscript and kind suggestions. The description in Line 202-209 is not accurate and it appears that the referee has some misunderstanding on what we did. In this study, we calculate the O^+/H^+ density ratio (as Figure 4b shown). The O^+ density calculated at energies from 1 keV to 40 keV, but the H^+ density (over the full HPCA energy range) from L2 data products are used. In order to realize in which individual energy ranges the O^+ abundance (O^+/H^+) varies obviously on AE index and solar wind parameters. We calculated the particle fluxes ratio at several individual energy ranges (as Figure 4c shown). Since the energy channel range of HPCA for H^+

and O^+ is the same, so the fluxes ratio are defined as the ratio between their fluxes, We also give the error bars indicating 90% confidence intervals. See Line 280-292 in "Tracked change" manuscript.

Comments 7: Line 218-248: Figures 5, 6, 7 all show comparisons of the O^+/H^+ density ratio. After addressing the previous comment on Line 202-209 on why separate narrow energy ranges were chosen instead of using a broad energy range, the authors may need to revise panel (b) of these three figures. For example on Line 240: Are the O^+ and H^+ densities referred to in this section calculated from one of the energy ranges discussed in Line 202-209? Greater detail and explanation are needed.

Response: It may be our inaccurate descriptions result in the referee's misunderstood. Figure 4b 5b, 6b, 7b show the O^+/H^+ density ratio used the broad energy range (as mentioned in Response to comment 6). While Figure 4c, 5c, 6c, 7c show the O^+/H^+ fluxes ratio at several individual energy ranges. We didn't calculate the O^+ or H^+ density from one of the energy ranges discussed in Line 202-209. So this relevant part of the description has been amended in my revised manuscript, see Line 277-285 in "Tracked change" manuscript.

Comments 8: Line 254-256: After addressing the above comments on how the ion densities were calculated, the authors should briefly address whether these comparisons of density across missions are relevant. For example, if the O^+ density (calculated over defined HPCA energy range) is higher than seen by Cluster (calculated in what energy range and using which instrument?), what does this mean? Were the instrument energy ranges equivalent or similar? Otherwise, the direct comparison may not be meaningful.

Response: Thanks for the referee's good evaluation and kind suggestion. This comment is very important. From Line 254-256, we can't exclude the reason that Bouhram et al., 2005 used somewhat different energy range for O^+ observations result in lower O^+ density in their study than mine. The direct comparison can't be meaningful. In this study, the O^+ density calculated using HPCA distribution functions at energies from 1 to 40 keV, but Bouhram et al., (2005) used CODIF distribution functions at energies from 3 to 40 keV to avoid contamination from high H^+ fluxes. The composition and distribution function (CODIF) analyzer on the Cluster that measures 3-D distributions of the major ion species over the energy range 30–40000 eV. This contrast study is not rigid in this study, so we removed the relevant part in our revised manuscript.

Comments 9: Line 305: Since 31 events are not a large number, recommend the authors produce a table to list the dates and times of each of these events so that others in the space science community can also investigate the events for follow-on studies. Such a table could go in an appendix.

Response: Yes, this is a good suggestion. I have prepared such a table to list the dates and times of each of these events for follow-on studies in an appendix (see the appendix).

Comments 10: All the references in the manuscript need to be checked. For example, all the MMS instrument papers were referenced but do not appear in the references list. It is likely any other references have been missed. It is likely many other references have been missed.

Line 106: Pollock et al. (2016) is referenced but does not appear in the references list
Line 105: Russell et al. (2016) is referenced but does not appear in the references list

Line 104: Ergun et al. (2016) is referenced but does not appear in the references list

Line 104: Lindqvist et al. (2016) is referenced but does not appear in the referenceslist

Line 107: Young et al. (2016) is referenced but does not appear in the references list

Response: Thanks for the referee's kind suggestion and carefully evaluating this paper. This mistake should have avoided in the manuscript submission. We added the MMS instrument papers citations in the references list. We also checked carefully all the references in the manuscript to make sure all the citations in the references list. The other spelling and syntax errors have also been checked and corrected in the revised paper.

Reply to reviewer #2

Dear reviewer:

We are very grateful to your comments for the manuscript and thanks for carefully evaluating this manuscript. According to your advice, we amended the relevant part of the manuscript. The one-to-one responses to your comments are the following.

Major comments

Comments 1:One of the conclusions of the manuscript is that particles are transported from the tail towards the dayside. To make such a conclusion more rigid one should show the anisotropy of the particle distributions, which would indicated that particles move from the tail towards the dayside. The oxygen ions could also come from other sources such as inner magnetosphere (filled directly from the nightside aurora into the ring current), from the diamagnetic cavities/cusp (e.g. Slapak et al., Ann. Geophys. 2013,10.5194/angeo-31-1005-2013).

Response: Thank you for pointing this out. Yes, the oxygen ions at the dayside LLBL have many sources such as the ring current in the inner magnetosphere, the high latitude auroral region and the cusp. Our paper focuses on the oxygen ions in the duskside magnetopause during intense substorms with AE >500nT. Previous research work has reported that the oxygen ions transferred faster into the ring current in the inner magnetosphere and then they are decayed at the dayside magnetopause under southward IMF or with their large gyroradius effect [e.g., Zong et al., 2001]. Under intense geomagnetic activities such as intense substorms and storms, the oxygen ions from the nightside aurora along the plasma sheet or plasma sheet boundary layer can be fast transferred into the near-Earth magnetotail and then injected into the ring current [e.g., Duan et al.,2017 JGR; Yu and Ridley,2013 JGR]. Recently, Kronberg et al. [2014] reported that the oxygen ions distribution was really anisotropic at the dawn-dusk equator plane. Our observation result is consistent with their report. I have to admit making such a conclusion is not rigid. Because we can't exclude other origins. I removed this expression in my revised paper.

Kronberg, E. A., Ashour-Abdalla, M., Dandouras, I., Delcourt, D. C., Grigorenko, E. E., Kistler, L. M.,…Zelenyi, L. M. (2014). Circulation of heavy ions and their dynamical effects in the magnetosphere: Recent observations and models. Space Science Reviews, 184(1-4), 173–235. https://doi.org/10.1007/s11214-014-0104-0

Yu, Y., and A. J. Ridley (2013), Exploring the influence of ionospheric O+ outflow on magnetospheric dynamics: dependence on the source location, J. Geophys. Res. Space Physics, 118, 1711–1722, doi:10.1029/2012JA018411

Zong, Q.-G., B. Wilken, S. Y. Fu, T. A. Fritz, A. Korth, N. Hasebe, D. J. Williams, and Z.-Y. Pu (2001), Ring current oxygen ions escaping into the magnetosheath, J. Geophys. Res., 106(A11), 25,541–25,556.

Comments 2:I am not sure if one could make firm conclusions about dependence on the IMF Bz,if from 31 events only 6 events were observed during northward IMF. On my opinion the statistics are too poor for that.

Response: Thank you for the comment. The events of energetic oxygen ions at the duskside magnetopause during intense substorms in our studies are chosen from MMS Phase 1. Because there are limited number of events of intense substorms when MMS passes through the duskside magnetopause during the Phase 1. So

the O$^+$ abundance dependence on IMF Bz is not clear. In the revision processes, We added the 26 event satisfied with the criterion into our work. Our work presents 57 intense substorms events with 50 events under the sourthward IMF Bz and only 7 events under the northward IMF Bz. The intense substorms are usually occurring duing southward IMF Bz .This is consistent with the usually external condition of intense substorms [Lyons et al., 2005]. On the other hand, We have added 26 events satisfied with the criterion in the revised paper for better study. We found the O$^+$ density shows expontial decrease with IMF Bz from -10 to 0 nT. This conclusion will be substitute with a more rigid expression in my revised manuscript. -->"When the IMF is southward, the O$^+$ density shows an exponential increase with the IMF Bz absolute value.", as shown in "Tracked change" manuscript Line 31-32.

Lyons, L. R., D.-Y. Lee, C.-P. Wang, and S. B. Mende (2005), Global auroral responses to abrupt solar wind changes: Dynamic pressure, substorm, and null events, J. Geophys. Res., 110, A08208, doi:10.1029/2005JA011089.

Comments 3: The "intense substorms" are discussed in this study. Were these substorms associated with magnetic storms? Or these are pure substorm events? What is the reason for choosing intense substorms? Inlcuding other substorms may increase the statistics on the IMF dependence.

Response: Thanks for the referee's kind suggestion. In this statistical study, 31 magnetopause crossing events during intense substorm (AE>500 nT) were selected. Among them, there are 4 events during the non-storm time (Dst> -25 nT) and 27 events during the storm time (Dst< -25 nT). There are three resons that we focused on investigating the characteristics of energetic oxygen ions at the duskside magnetopause during intense substorms. Firstly, previous studies have reported that the density and energy flux of oxygen ions in the magnetosphere both increased during magnetic activities, such as intense substorm and storms (e.g.,Daglis et al.,1994; Kronberg et al.,2014). During During disturbed times, oxygen ions can be energized due to duskward drift along the dawn- dusk eletric field in the course of their covection from the distant tail towards the Earth. And the oxygen duskward asymmetry is observed at the near-Earth nightside (eg. Nosé et al., 2000; Luo et al., 2014). So l want to realize the relations between magnetail processes with the Oxygen abundance in the duskside magnetpause. Second, Oxygen ions play a significant role in the energy and mass transport in the coupling process of the solar wind-magnetosphere-ionosphere during intense substorms. The responses of energetic oxygen ions at the duskside magnetopause boundary layer to the solar wind conditions during intense substorms have seldom be reported till now. Third, MMS project can provide a good chance to investigate the features of energetic oxygen ions in the dayside magnetopause boundary layer. The previous spacecraft observations provided significant results of oxygen ions mainly focusing on the tail plasma sheet or middle and high latitude region, such as Cluster [e.g., Nilsson et al.,2006;Slapak et al.,2011]. Thus, our investigation can provide new results in the duskside magnetopause.

Daglis, I. A., Livi, S., Sarris, E. T., & Wilken, B. (1994). Energy density of ionospheric and solar wind origin ions in the near-Earth magnetotail during substorms. Journal of Geophysical Research, 99(A4), 5691–5703. https://doi.org/10.1029/93JA02772

Kronberg, E. A., Ashour-Abdalla, M., Dandouras, I., Delcourt, D. C., Grigorenko, E. E., Kistler, L. M.,...Zelenyi, L. M. (2014). Circulation of heavy ions and their dynamical effects in the magnetosphere: Recent observations and models. Space Science Reviews, 184(1-4), 173–235, doi:10.1007/s11214-014-0104-0.

Ono, Y., M. Nosé, S. P. Christon, and A. T. Y. Lui (2009), The role of magnetic field fluctuations in nonadiabatic acceleration of ions during dipolarization, J. Geophys. Res., 114, A05209, doi:10.1029/2008JA013918.

Luo, H., E. A. Kronberg, E. E. Grigorenko, M. Franz, P.W. Daly, G. X. Chen, A. M. Du, L. M. Kistler, and Y.Wei (2014), Evidence of strong energetic ion acceleration in the near-Earth magnetotail, Geophys. Res. Lett., 41, 3724–3730, doi:10.1002/2014GL060252.

Nilsson, H., et al. (2006), Characteristics of high altitude oxygen ion energization and outflow as observed by Cluster: A statistical study, Ann. Geophys., 24, 1099–1112.

Slapak, R., Nilsson, H., Waara, M., André, M., Stenberg, G., and Barghouthi, I. A.(2011), O+ heating associated with strong wave activity in the high altitude cusp and mantle, Ann. Geophys., 29, 931–944, doi:10.5194/angeo-29-931-2011

Comments 4: Introduction, first two paragraphs can be merged as they contain repeating information about acceleration during dipolarizations. The second paragraph is not completely logical. It would make more sense to describe acceleration of O^+ starting from the polar region, then lobe, dipolarizations and then discuss drift. The sentence in lines 43-45 discussing acceleration of electrons during dipolarizations is not really needed as there is a number of references about acceleration of oxygen during dipolarizations in lines 29-47 and the whole text is about O^+.

Response: Thanks for the referee's kind advice. As you suggested, I adjusted the description order in seconde paragraph to make the introduction more logical and concise.The part of revision can be found in Line 40-65 in "Tracked change" manuscript.

Comments 5: lines 90-91, "At present, O^+ near the dayside low-latitude magnetopause during substorm expansion phase and recovery phase are still not understood" –> What exactly do you mean under not understood? Which scientific questions are still open? Which questions do you try to answer?

Response: Thank you for these comments. Actually, what we want to know is how the O^+ abundance (O^+/H^+) in the duskside magnetopause varies on AE index and solar wind conditions (e.g. IMF By, IMF Bz, and solar wind dynamic pressure) during the intense substorm (AE >500 nT).The relevant description is revised in "Tracked change" manuscript Line 114-117.

Comments 6: lines 91-93, there is paper by Luo et al., JGR, 2017, 10.1002/2016JA023471, in which the energization of O^+ at the dayside is discussed. The study also discusses asymmetries of the energetic oxygen due to IMF By and Bz directions. Both IMF By and Bz influence the oxygen abundance at higher energies. However, this is large statistical study and not only cases for the intense substorms. This can be discussed.

Response: That would be great. We discussed Luo et al., (2017) results in my revised manuscript. The relevant part can be found in "Tracked change" manuscript Line 399-402. Recently, Using energetic ion

composition data at the low latitude dayside magnetopause measured by Magnetospheric Multiscale (MMS) satellites, we study the response of O^+abundance (O^+/H^+) to the both IMF By and Bz and not only cases for the intense substorms. We found that they indeed influence the oxygen abundance even at lower energies (1-40 keV) and more significant duskside asymmetry of O^+ under southward IMF with positive IMF By. These results are consistent with those of Luo et al.,(2017).

Comments 7: lines 125-126, 130-131, 180-181, please provide a more precise definition of the substorm onset and recovery phase. For example in paper by Newell and Gjerloev, JGR, 2011, 10.1029/2011JA016779, is a nice example on how to define substorm onset, also using more precise SML index available at the SuperMAG. I do not think that definition when "AE index significantly increases" is a precise one. I do not think that one should provide twice the information about substorm onset in lines 125-126 and 130-131. I would remove the second sentence.

Response: Thanks for constructive comments and nice recommendation. We have added a more precise definition of the substorm onset, expansion phase and recovery phase in our revised manuscript. The second information about substorm phase description in lines 125-126 and 130-131 has been removed. We added AU, AL index in Figure 1 to help us identify the phase of a substorm. First, we determined the time interval of the magnetopause boundary layer crossings in each event. Then, we find out how the substorm indices change during that interval from the OMNI data. As Figure 1 shown, the time interval of the magnetopause boundary layer crossing is indicated by the two blue dashed lines. As we know, the AE index is defined as AE=AU-AL. Generally,the substorm onset time is characteristic by the AL index starts to significantly decrease and the AE index significantly increase. During the substorm expansion phase, the AL index will decrease significantly. The interval of the AL index decrease from onset to its minimum is defined as the substorm expansion phase. Then it starts to increase and the interval of the AL index increase from the minimum to the quiet time level is regarded as the substorm recovery phase. In our event, the MMS4 crossed the magnetopause boundary layer from 15:25:10 to 15:36:50 UT on 3 October 2015. From Figure 1f, the AL index reached its minimum ~-750 nT and AE index reach the peak ~1000 nT at about 15:20 UT, then it started to increase to ~ -200 nT at the rest time of interest. So the magnetopause boundary layer crossing occurred during the intense substorm recovery phase. (see Line 167-180 in "Tracked change" manuscript)
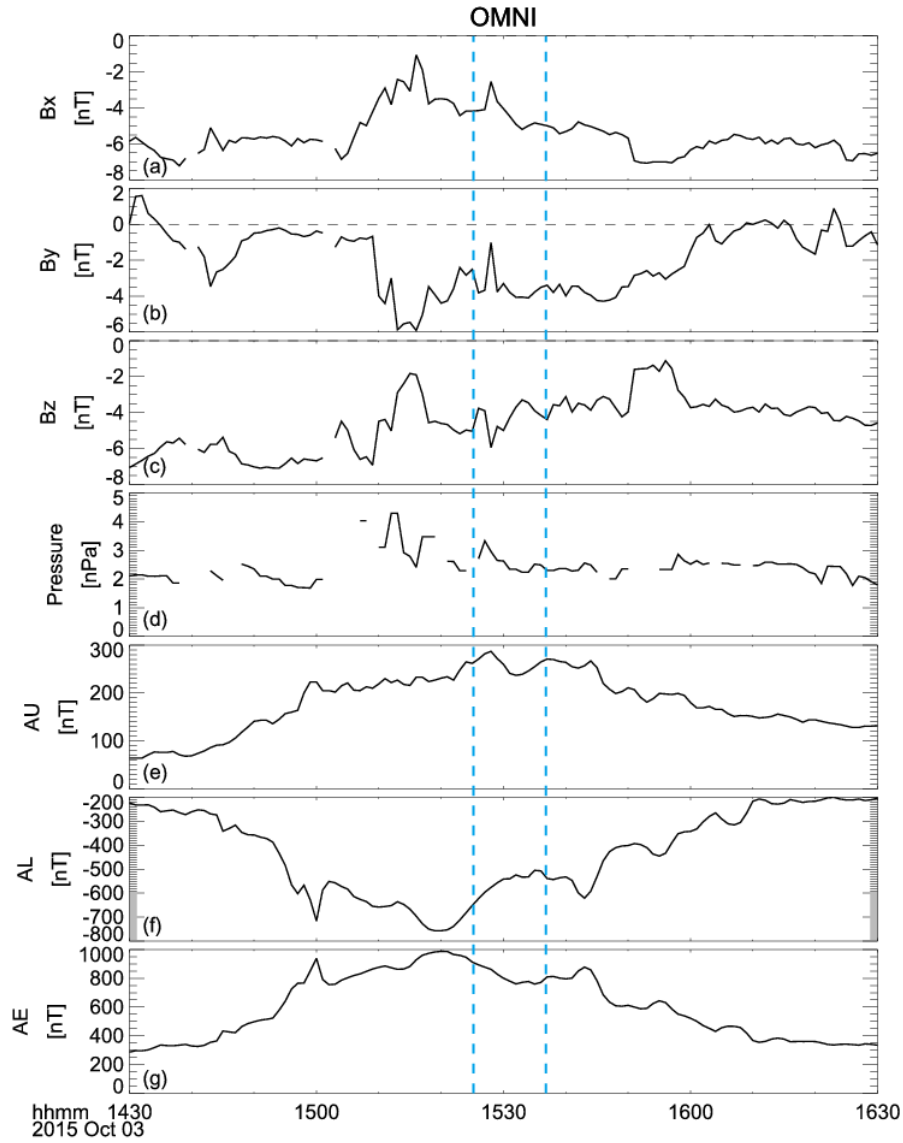
Figure 1. The three components IMF Bx, By, Bz, solar wind dynamic pressure, as well as AU, AL, and AE index from CDAweb OMNI data.

Comments 8: lines 179-180, actual observations of the IMF and solar wind dynamic pressure could be used directly from the MMS observations at the magnetopause crossings. This would be much more precise.

Response: Getting the much more precise IMF and solar wind dynamic pressure would be better. When the IMF passes through the bow shock, its direction would be changed in the magnetosheath. We will compare

the IMF and solar wind dynamic pressure directly from the MMS-with those from OMNI data in the detailed events analysis. Then we will choose the more precise data.

Comments 9: lines 277-278, For higher energies the larger statistics one can clearly see that the stronger duskward asymmetry in the plasma sheet and the dayside magnetosphere is observed under the southward IMF, e.g. Luo et al., JGR, 2017. One should mention that no influence of IMF Bz is observed in case of the energies below 40 keV and for 31 intense substorm events.

Response: Thanks for your constructive suggestion. We agree with your comments. Recently, We used energetic ion composition data at the dayside magnetopause measured by Magnetospheric Multiscale (MMS) satellites, we study the response of O^+ abundance to IMF Bz. The O^+ abundance showing strong duskside asymmetry in the magnetopause boundary layer under southward IMF than that under northward IMF also be found in our study, which is consistent with Luo et al.2017 result. As you suggested, the influence of IMF Bz is not clear in our 31 intense substorm events. This description in Lines 277-278 has been removed.

Comments 10: lines 286-287, the energetic O^+ occurs predominantly under southward IMF. Here I would say that it was chosen to be like this. Choosing the intense substorms one increases the probability of observing the southward IMF quite significantly. This also contradicts to statement in the lines 277-278, that IMF Bz does not influence abundance of O^+ at the magnetopause. There is not enough provided data to conclude so. By increasing the number of events under the northward IMF one may see a different picture. One can see pretty nice trend in Figure 6b, that the abundance is increasing with the decrease of IMF Bz at least for the expansion phase. Generally on my opinion there is not enough statistics in this study to make conclusions about IMF dependence. One should expand the statistics

Response: Thanks for your valuable comments. We agree with you that choosing the intense substorms one increases the probability of observing the southward IMF significantly. To make convincing conclusions about IMF dependence, we expanded the statistic to 57 events. Some conclusions may be still not convincing due to not enough statistical events. As the MMS operate longer, more magnetopause crossing during intense substorm will be detected. It will be helpful. The sentences in Line 286-287 have been deleted.

Comments 11: lines 304-306, this conclusion is not supported by the observations. Just looking at the scatter points of the number density, I do not see a statistically significant difference between these two phases. One should either show fits to those points or bin them according to some parameters and show that the difference is significant.

Response: Thanks for your comments. At the beginning of this study, we focus on the response of O^+ abundance on the geomagnetic activity and solar wind conditions during intense substorms. Because the magnetosphere has the different dynamics in the near-Earth space during the different phase of intense

substorms, especially in substorm expansion phase and recovery phase. So we want to investigat variations of energetic O⁺ density at the duskside magnetopause boundary layer duing different phases of intense substorms. Due to the number of events are limited (only 26 events during expansion phase), we don't think it makes sense to fit those points or bin then according to some parameters. As the MMS operating longer, more magnetopause crossing during intense substorm will be detected. It will be helpful. Our selecting events we drawn our summary on the energetic O⁺ density as description in the last part of our manuscript. In generally, the O⁺ in the magnetosphere are origin from the ionosphere and transferred into the different magnetosphere region during magnetic activities. A excellent review paper of this aspect has been reported by Keika et al., (2013). Our new results from MMS data provide another support of previous studies.

Keika, K., L. M. Kistler, and P. C. Brandt (2013), Energization of O+ ions in the Earth's inner magnetosphere and the effects on ring current buildup: A review of previous observations and possible mechanisms, J. Geophys. Res. SpacePhysics, 118, 4441–4464, doi:10.1002/jgra.50371.

Comments 12: lines 313-315, energetic oxygen ions also indicate the transport at the dayside magnetosphere (e.g. Liao et. al, JGR, 2010, 10.1029/2010JA015613). These different transports are hard to distinguish (e.g. Luo et al., JGR, 2017).

Response: Thanks for your comments and paper recommendation. Liao et al., (2010) JGR and Luo et al.,(2017) JGR are both cited in our revised manuscript (see see Line 391-397 and Line 399-402 in "Tracked change" manuscript). I agree with you, these different transports are hard to distinguish. Also, the different transports of oxygen ions from the ionosphere to different part of the magnetosphere are significant and interest. It is outside the focus of our manuscript. We will investigate this issue with conjunction observations by multiple spacecraft in different magnetosphere locations. This conclusion in Line 313-315 has been deleted.

Comments 13: Figures 4-7, just looking at the scatter plots it is hard to make certain conclusions.One should either bin the points to show the average trend or fit them with some dependences and increase the number of events.

Response: Thanks for your nice suggestions. I have binned the points to show the average trend before submitted this manuscript. As you said,the number of events is too low, so the trend is not obviously or has low credibility and we abandoned this method. As you suggested, we fit the oxygen density dependence on the IMF Bz and Psw, respectively. Recently, Using energetic ion composition data at the low latitude dayside magnetopause measured by Magnetospheric Multiscale (MMS) satellites, we study the response of H⁺, O⁺density and their ratio to the geomagnetic activity (indicated by SYM-H index) and solar wind conditions (including interplanetary magnetic field (IMF) By, IMF Bz and solar wind dynamic pressure). In this study, we bin the points due to enough events. Our new manuscript has been submitted to the JGR.

Minor comments:

1. **Line 19:** What is the energy range of the oxygen observations used in this study? Please indicate the upper energy limit in the abstract. This is important to know when assessing the number densities.

Response: In this study, only the O^+ at energies from 1 keV to 40 keV measured by HPCA are used. The upper energy limit of HPCA is 40 keV. This information is added to the abstract. (see Line 18 in "Tracked change" manuscript)

2. **Line 45:** I did not find the reference to Lui et al., 1999 in the reference list. (see Line 589-591 in "Tracked change" manuscript)

3. **Line 47:** "during activity geomagnetic disturbance" –> "during disturbed geomagnetic activity" (see Line 50-51 in "Tracked change" manuscript)

4.**Line 55:** "[e.g. Yau and Andre, 1997]. And then..." –> "[e.g. Yau and Andre, 1997] Then..." (see Line 62 in "Tracked change" manuscript)

5.**Line 85:** please remove one "However". (see Line 109 in "Tracked change" manuscript)

Response to comments from 2-5: The above expression errors have been checked and corrected. The missing reference has been added to the revised manuscript.

6. **Lines 106-107**: Does HPCA distinguish between O^+, N^+, and C^+? Or what measures actually the CNO group?

Response: "the HPCA is a time-of-flight (TOF) mass spectrometer designed to measure the velocity distributions of the four ion species (H^+, He^{++}, He^+ and O^+) known to be important in the reconnection process. The measurement technique is based on a combination of electrostatic energy-angle analysis with time-of-flight velocity analysis. The result is an accurate determination of the velocity distributions of the individual ion species. In order to meet the stringent scientific requirements of the MMS mission, the HPCA incorporates three new technologies. The first extends counting rate dynamic range by employing a novel radio frequency mass filter that allows minor species such as He^{++} and O^+ to be measured accurately in the presence of intense proton fluxes found in the dayside magnetopause. The second ensures that TOF processing rates are high enough to overlap with the low end of the RF dynamic range, while the third enhances ion mass resolution.

Fig. 20 TOF spectrum for four ion species and background (H_2^+ is a substitute for He^{++} and N^+ is a substitute for O^+). *Red areas* demarcate bins that define ion species and background. The *peak* at ~200 ns corresponds to N_2^+
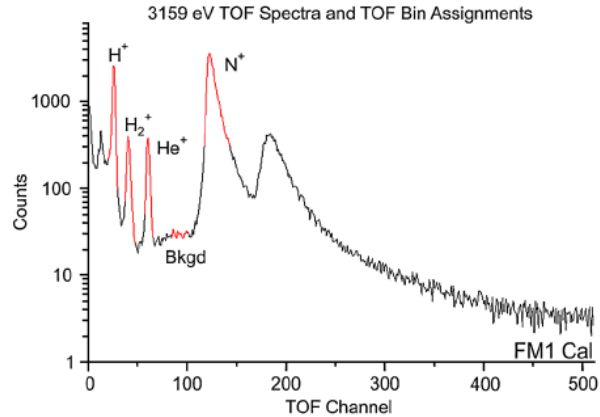
Fig. 31 TOF boundaries as a function of energy for four ion species plus background
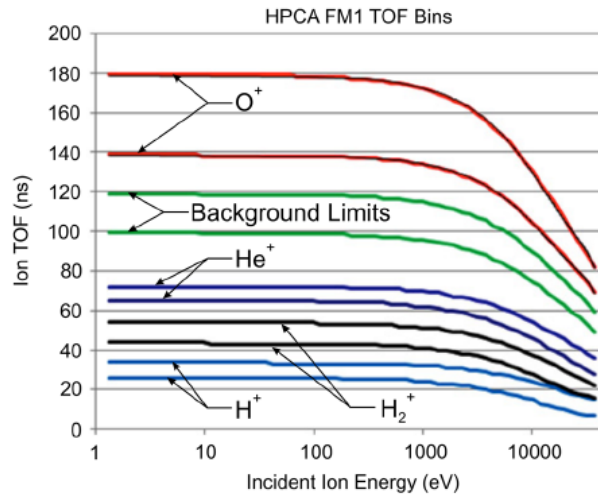
During each energy scan a data set consisting of 63 TOF spectra × 512 TOF bins × 16 elevations is accumulated and histogrammed. The resulting TOF spectra are then parsed into five bins that define the ion species H+, He++, He+, O+ and background (Fig. 20). The red portions of the spectrum in Fig. 20 indicate typical species boundaries. Since ion times-of flight are both mass and energy-dependent the range of TOF limits for each species changes with energy (Fig. 31)". (the Figure and description are cited from Young, D. T., Burch, J. L., Gomez, R. G., De Los Santos, A., Miller, G. P., Wilson, P., et al. (2016). Hot Plasma Composition Analyzer for the Magnetospheric Multiscale Mission. Space Science Reviews, 199(1–4), 407–470, doi:10.1007/s11214-014-0119-6.).

As for this interesting question, I specially contacted the HPAC PI (Stephen Fuselier), he replied me "**I'm working right now to see if we can see C+ and possibly N+ in the mass spectra. They would not appear as a separate mass peak because of straggling in the foil. I'm not sure if we can even tell if they are there. What we bring to the ground and call O+ could contain substantial N+. The C+ peak would probably be at a lower time-of-flight than what we bring to the ground, but you could safely say that what we call O+ could be N+O+.**"

7. **Line 122:** "At the beginning of the time interval, the solar wind dynamic pressure..."–>The dynamic pressure is only at the begging of the time interval about 2 nPa. (see Line 161-162 in "Tracked change" manuscript)

8. **Lines 124-125**: I would change to " These solar wind conditions led to the intense substorm (AE>500 nT). (see Line 166 in "Tracked change" manuscript)

9. **Lines 148-150:** Figure 2, I would say that the fluxes at energies below 2 keV in Figure 2j is also contamination. This should be mentioned also in Figure caption and even better when it is indicated on the plot itself. (see Figure 2j red box in revised manuscript)

Response to comments from 7-9: Thanks for the referee's valuable suggestion. The minor comments 7 and 8 have been corrected in my manuscript. The red box indicating the O^+ contamination from high proton fluxes was plotted in figure 2j and relevant description was mentioned in the Figure 2 caption (see Line 676-677).

10. **Line 195:**I would remove "On the other hand".

Response: This is a common colloquial expression. We removed it.

11. **Lines 221-224:** These results also agree with Kronberg et al., JGR, 2012,10.1029/2012JA018071 which showed for 10 keV O^+ strong increasing under the duskward IMF indicated by the clock angle in the inner magnetosphere.

Response: That would be great. We cited this paper in the relevant part of the revised manuscript to increase valid of our results. see Line 387-389 in "Tracked change" manuscript)

12. **Lines 251-268:** another reason can be that *Bouhram et al.,* 2005 have used somewhat different energy ranges for O^+ observations.

Response: Yes, We agree with you. I can't exclude the reason that *Bouhram et al.,* 2005 used somewhat different energy range for O^+ observations. In this study, the O^+ density calculated using HPCA distribution functions at energies from 1 to 40 keV, but Bouhram et al., (2005) used CODIF distribution functions at energies from 3 to 40 keV to contamination from high H^+ fluxes. This contrast study is not rigid in this study. We removed the relevant part in my revisited manuscript.

13. **Line 276:**magenetopause –> magnetopause.(see Line 384 in "Tracked change" manuscript)

14. **Line 279:** have –> has. (see Line 390 in "Tracked change" manuscript)

15.**Line 287:** dominated occurring –> occurs predominantly.(removed)

17. **Lines 296-297:** I would change this sentence to "The reconnection rate is likely will be reduced by the mass-loading but not suppressed at the magnetopause [*Fuselier et al.,* 2019]. (see Line 429-430 in "Tracked change" manuscript)

17. **Figure 1**, caption, "The three components of the IMF, Bx, By, Bz..." (see Line 661 in "Tracked change" manuscript)

18. **Figure 2,** I would indicate on the plot contamination. In the caption, line 481 (k)–>(l). (see Line 671 in "Tracked change" manuscript)

Response to comments from 13-18: Thanks for referee'scarefully evaluating this paper and important suggestions. We have revised the above errors and plotted the red box indicating the O^+ contamination from high proton fluxes in figure 2j. The other spelling and syntax errors have been checked and corrected. We acknowledge the reviewer's comments and suggestions very much, which are valuable in improving the quality of our manuscript.

Reply to reviewer #3

Comments 1: Lines 90-95: There is a lot of information leading up to this point in the introduction, however with the lines preceding and in this paragraph itself, it is unclear what is not well understood and how/what this paper will provide to answers to. Currently, the introduction reads as a quite thorough list of previous studies, but it is not readily apparent how they string together, and what they are necessarily building up to. I would suggest stating what the paper will study before this point and tailoring the introduction to build off of that somewhat, because at this point as a reader it is still unclear.

Response: Thanks for the referee's kind advice. As you suggested, we did some revisions in our revised manuscript. We adjusted the first two paragraphs to make the introduction more logical and concise (see Line 40-65 in "Tracked change" manuscript). The introduction is organized as following orders. First, we stress the importance of O^+ during the intense substorms, describe acceleration of O^+ starting from the polar region, then lobe, near-Earth plasma sheet and then discuss drift. Second, we describe the O^+ behavior in the magnetopause. Third, we referred to the O^+ density dawn-dusk asymmetry in the magnetopause. Finally, we describe the questions what this paper tries to answer. As the following described: "At present, variations of O^+ abundance (O^+/H^+) in the dusk flank magnetopause during intense substorms (AE >500 nT) on AE index and solar wind conditions (e.g. IMF By, IMF Bz, and solar wind dynamic pressure) are still not understood. Previous studies of O^+ during intense substorms mainly focused on O^+ energizations in the NEPS in the magnetotail (e.g., Duan et al., 2017; Nosé et al., 2000; Ohtani et al., 2011). At present, The Magnetospheric Multiscale (MMS) mission gives us an opportunity to focus on the O^+ in the low latitude dayside magnetopause region. In this study, we mainly investigate statistical features of energetic O^+ in the dusk flank magnetopause and their relations with AE index and solar wind conditions (e.g. IMF By, IMF Bz and solar wind dynamic pressure) during the intense substorms. (see Line 114-124 in "Tracked change" manuscript)

Comments 2: Lines 128-150: HPCA & FPI fluxes are in differential flux and energy flux units. Is there a benefit in having their fluxes in different units? If they are to remain, a point should be included in the text that the units are different.

Response: Thanks for the referee's kind suggestion. We described the HPCA and FPI fluxes having different units in our revised manuscript. Figures 2g and 2h show the electron omnidirectional differential energy fluxes and ion omnidirectional differential energy fluxes, respectively. Figure 2i to 2l presents the differential particle fluxes of H^+, O^+, He^+, He^{++}, respectively. To better identify the fluxes variations at specific energies, we choose the ion and electron fluxes from FPI in the energy flux unit. The relevant description has been add into the Line 195-198 in "Tracked change" manuscript)
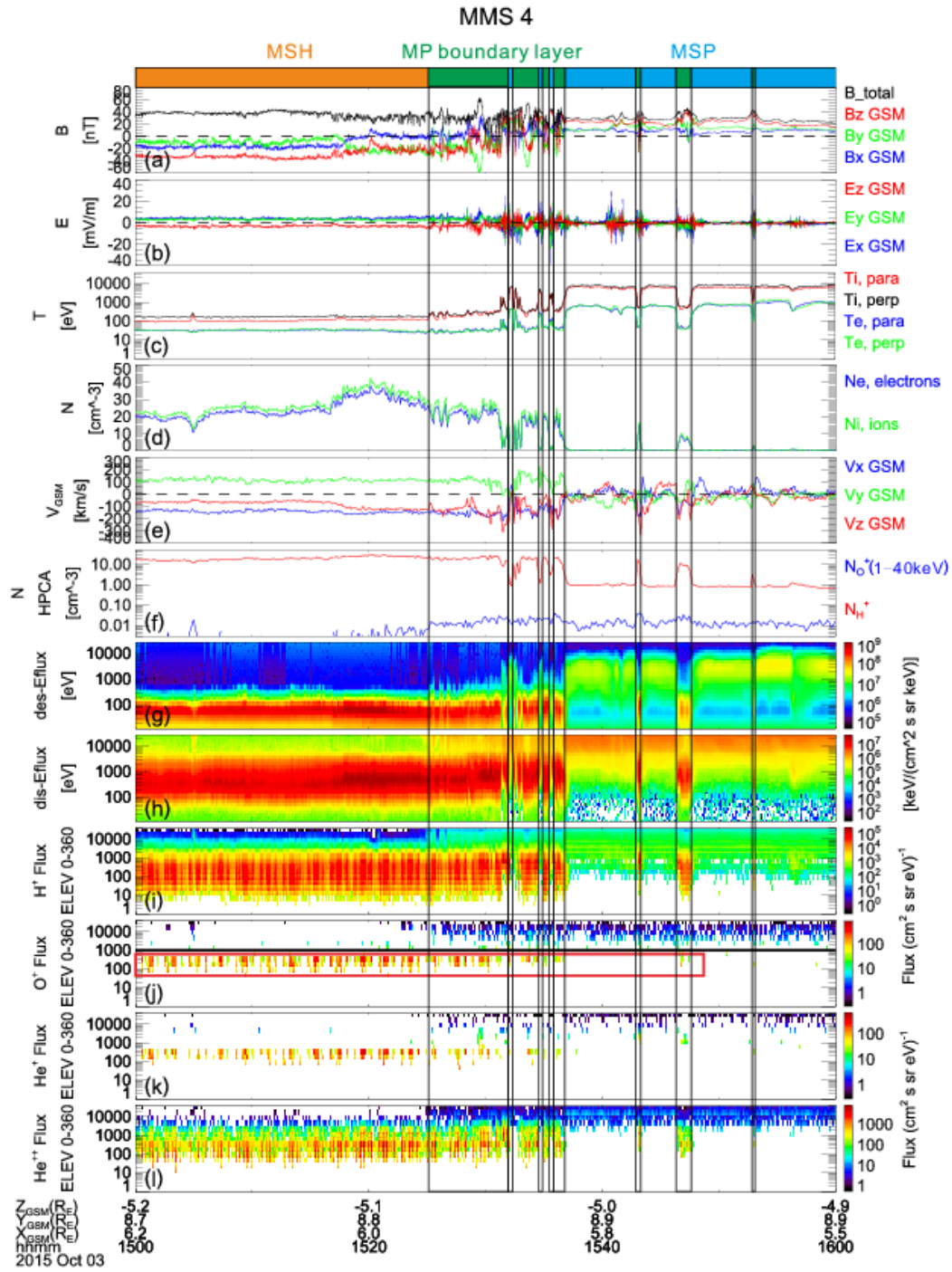
Figure 2. The energetic O⁺ is observed at the magnetopause during an intense substorm on 03 October 2015 by MMS 4. From top to bottom are (a) the magnetic field three components, Bx (blue line), By (gree line), Bz (red line) and the total magnitude Bt (black line), (b) the electric field three components, Ex (blue), Ey (gree) and Ez (red), (c) Ion parallel (red) and perpendicular(black) temperatures, (d) The density of ion (green) and electron (blue), (e) three components of the ion velocity, (f) the H⁺(overthe full HPCA energy range) and O⁺ (at energies from 1 to 40 keV)densities, (g) electron omnidirectional differential energy fluxes, (h) ion omnidirectional differential energy fluxes,(i) to (l) present differential particle fluxes of H⁺, O⁺, He⁺, He⁺⁺, respectively. The Geocentric Solar Magnetospheric (GSM) coordinate system is adopted. The thick bars at the top of the panel present different regions encountered

on this magnetopause crossing event. The orange and blue bars represent the magnetosheath and the magnetosphere, respectively. The green bar represents the magnetopause boundary layer. The black horizontal line in figure 2j is at 1keV and the O^+ contamination from high H^+ fluxes is indicated by the red box. The FPI data in Figure 2(c-e) and (g-h) are from FPI L2 data products and in the fast mode.

Comments 3: Lines 128-150: The HPCA flux in panels i-l have artificial striping every 4 energy bins due to way HPCA determines the count rate over 4 energy channels in survey mode. It would be best to correct this, however, describing the artificial striping would also be sufficient. I am also not certain that these HPCA fluxes are actually omni-directional as they do not appear to be half-spin averaged, please verify.

Response: Thanks for your important comments. "The HPCA flux in panels i-l have artificial striping every 4 energy bins due to way HPCA determines the count rate over 4 energy channels in survey mode." The above sentence has been added into the Line 194-195 in "Tracked change" manuscript. Figure 2i to 2l presents the differential particle fluxes of H^+, O^+, He^+, He^{++}, respectively. They are actually not Omni-directional and not half-spin averaged. We corrected this description in our revised manuscript. These differential particle fluxes of H^+, O^+, He^+, He^{++} calculations are used The Space Physics Environment Data Analysis System (SPEDAS) software package. More details about SPEDAS can be found in Angelopoulos et al. (2019) and cited as (Angelopoulos, V., Cruce, P., Drozdov, A. et al. Space Sci Rev (2019) 215: 9. https://doi.org/10.1007/s11214-018-0576-4). We also cited this paper in our revised manuscript (see Line 478-479 in "Tracked change" manuscript).

Comments 4: Lines 134-137: Please describe where the FPI/HPCA moments shown come from. This is quite important since the majority of the results presented are dependent on these moments.

Response: Thanks for the referee's kind advice. We have clarified where the FPI/HPCA moments shown come from. We have added detailed information about moments into Line 198-207 in "Tracked change" manuscript. The plasma moments (e.g. Ion parallel and perpendicular temperatures, ion, and electron densities and ion velocity) from FPI shown in Figure 2c-e are all from MMS L2 data products. They are default moments calculated over the full FPI energy range from 10 eV to 30 keV. But the O^+ density shown in Figure 2f is recalculated from HPCA distribution functions in the range of energies from 1 to 40 keV. From the O^+ fluxes shown in Figure 2j, there still exist a large number of fluxes below 1 keV in the magnetosheath. This part of O^+ fluxes is fake and contamination from high proton fluxes. So we consider the number density of O^+ with energies from 1 to 40 keV. It is more appropriate to represent the true O^+ in the magnetopause. While the H^+ density which computed over the full HPCA energy range from 1eV to 40 keV from L2 data products are used in Figure 2f.

Comments 5: Figures 1-2: I would suggest using these two figures to establish the criteria for the statistical study. In my opinion, more text should be added that describes a greater context for these 2

figures inclusion. Either establishing points that lend themselves to the paper's conclusion and/or use the figure to establish conditions for the statistical study.

Response: Thanks for your nice comments. In this statistical study, First, we identified the magnetopause crossing event (complete magnetopause crossing from the magnetosheath to the magnetosphere, vice versa) during phase 1 from the summary plot in https://lasp.colorado.edu/mms/sdc/public/plots/. Then we plotted the more detailed overview of these events to identify the magnetopause boundary layers, as Figure 2 shown. Figure 2 was mainly used to determine the magnetopause boundary layer crossing interval. Only events that AE index larger than 500 nT during the magnetopause boundary layer crossings interval were selected. Finally, the mean value of the H^+, O^+ density and their fluxes shown in Figure 2 were calculated in the magnetopause boundary layer. Correspondingly, the AE index, IMF By, Bz and solar wind dynamic pressure from the OMNI data system shown in Figure 1 were also averaged during that interval. Figure 1 mainly provided the corresponding solar wind conditions and AE index. The above expressions have been added into Line 245-256 in the "Tracked change" manuscript.

Comments 6: Lines 176-181: This is one of the more major comments on the paper. The current description of the event selection criteria is not sufficient. Interpretation of a statistical study is almost entirely dependent on understanding how the statistical study is conducted. It is currently not clear what the criteria for event selection is. Is it any MP crossing with AE > 500? Why was 500 chosen as a threshold in AE (i.e. stats are somewhat low, would AE > 300 or 400 provide more events and still be "intense"?).

Response: Thanks for your valuable comment. The magnetopause crossing event in our statistical study all during the intense substorm (AE > 500nT). How we chose these events is replied in the before comment. The reason why we choose intense substorm with AE >500 nT is based on the results from Daglis et al (1994) (Figure 6 in this reference, as shown in the below). They found that the O^+ energy density has a great correlation with the AE index in the near-Earth plasma sheet (NEPS). During the intense substorm expansion phase, O^+ energy density explosively increases with AE index in the range of larger than 500nT. Otherwise, Lennartsson and Shelley, (1986) pointed out that the ion composition had a large variance at substorm. During the intense disturbed conditions (AE~1000nT), the increase in the O+ energy density is strongest around local midnight where O^+ become the most abundant ion. The previous researches of oxygen ions during intense substorms are mainly focused on the nightside NEPS. Thus, we want to know whether the O^+ abundance in the dusk flank magnetopause varies on AE index and solar wind conditions during the intense substorm and how it changes with the above parameters. Characteristics of Oxygen ions in the high latitude polar region and near-Earth magnetosphere during

intense magnetic activities have been investigated deeply and widely. But O^+ abundance in the dayside magnetopause has seldom been reported during intense substorms.

Ion energy density at substorm expansion-phase
AMPTE/CCE - CHEM spectrometer (58 events)
Exponential fit: b=2.23x10⁻³, a=0.16, r=0.37, F=9.12

Figure 6. Same format as Figure 2; all substorms with $AE_{exp} \geq 500$ nT (encircled symbols) are excluded from the fit.
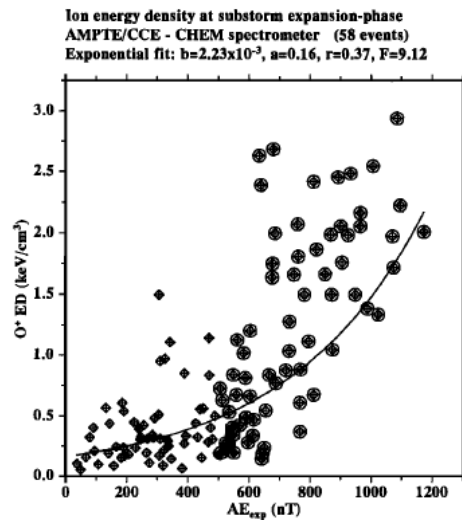
Comments 7: How exactly is the magnetopause boundary layer determined? Is there any consideration for if the substorm is during a storm or the 1st/2nd/3rd in a series of substorms? Specifically, how are substorm phases determined? What is meant by the mean value of the flux (over a range of energies, one energy)? How long were the average events? Please provide greater context for the choices of criteria used in this study.

Response: The magnetopause boundary layers are identified here primarily through plasma fluxes and moments. The magnetopause boundary layer can have densities and temperatures between that of the magnetosphere and the magnetosheath. Meanwhile, the magnetopause boundary layer shows the gradient of the energy flux of particles and number density and magnetic field obvious. Ion jets are also signatures of passing through the magnetopause boundary layers. In this study, the separatrix between the magnetosheath and the magnetopause boundary layer is determined by the appearance of the magnetospheric electron. Similarily, the separatrix of the magnetosphere and the magnetopause boundary layer is determined by the magnetosheath electron disappearance. The mean value of the H^+, O^+ density and their fluxes are calculated in the magnetopause boundary layer. Correspondingly, the AE index, IMF By, Bz and solar wind dynamic pressure from the OMNI data system were averaged during the time interval of magnetopause boundary layer crossing. As Figure 2 shown, the time interval of the magnetopause boundary layer crossing is marked by the two blue dashed lines. As we know, the AE index is defined as AE=AU-AL. Generally, the substorm onset time is characteristic by the AL index starts to significantly decrease and the AE index significantly increase. During the substorm expansion phase, the AL index will decrease significantly. The interval of the AL index decrease from onset to its minimum is defined as the substorm expansion phase. Then it starts to increase and the interval of the AL index increase from the minimum to the quiet time level is regarded as the substorm recovery phase. In our event, the MMS4 crossed the magnetopause boundary layer from 15:25:10 to 15:36:50 UT on 3 October 2015. From Figure 1f, the AL index reached its minimum ~-750 nT and AE index reach the

peak ~1000 nT at about 15:20 UT, then it started to increase to ~ -200 nT at the rest time of interest. The two blue dashed lines indicate the time interval of the magnetopause boundary layer crossing. According to the variation and peak value of the AU, AL and AE index in Figure 1e to 1g.The magnetopause boundary layer crossing occurred during the recovery phase of this intense substorm. The mean value of the flux is over two energy ranges close to the typical energy such as 1 keV, 10 keV and etc. We didn't consider if the substorm in during a storm or the 1st/2nd/3rd in a series of substorms. In this statistical study, 31 magnetopause crossing events during intense substorm (AE>500 nT) were selected. Among them, there are 4 events during the non-storm time (Dst> -25 nT) and 27 events during the storm time (Dst< -25 nT).These detailed contexts for choices of criteria used in this study are described Line 246-250 in the "Tracked change" manuscript.
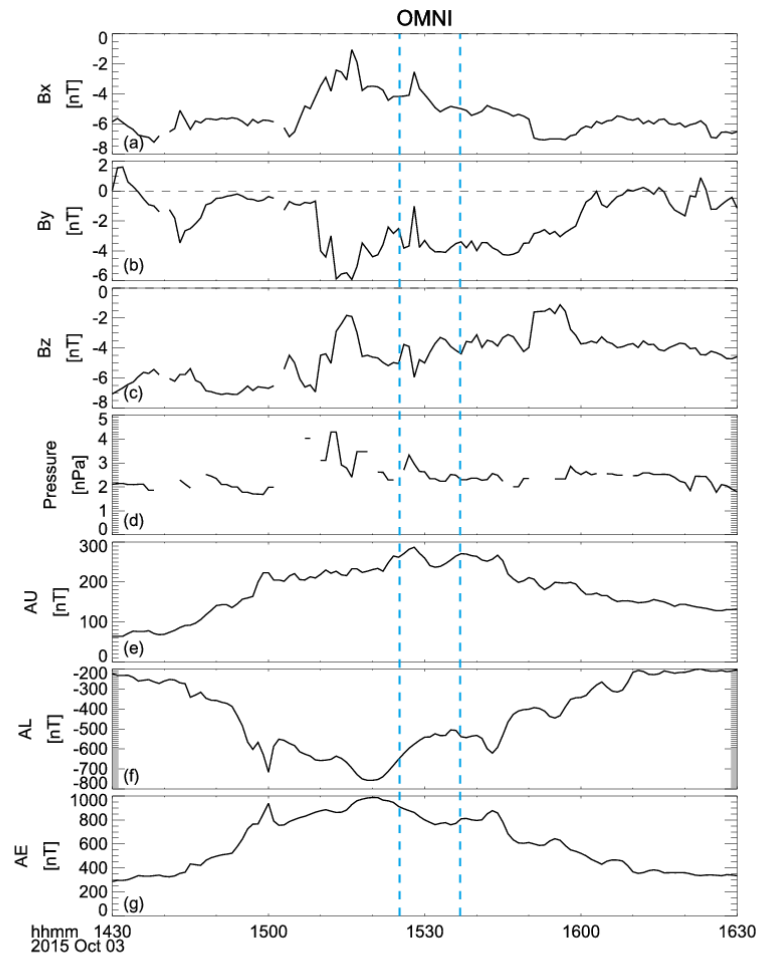
Figure 1. The three components of the IMF Bx, By, Bz, solar wind dynamic pressure, as well as AU, AL, and AE index from CDAweb OMNI data.

Comments 8: Lines 179-180: One of the main points from this paper is that the high-density O^+ can be transported from the nightside tail to the magnetopause where it is observed. Please discuss any effect

(or lack there of) of using OMNI solar wind values at the bow shock to correlate with observations of high O^+ density which is being driven by processes which invariably take some amount of time to occur.

Response: Thanks for the referee's good evaluation and kind suggestion. Making such a conclusion is not rigid. I didn't give direct evidence to prove that these O^+ are transported from the tail towards the dayside. So, I deleted this expression in my revised paper.

Comments 9: Lines 203-205: With the decimation of HPCA fluxes during survey mode, the count rate is recorded/distributed over 3-4 energy channels. With this in mind, is it appropriate to describe the comparisons of the flux as being over such a small energy range, since the flux/count rate could have been dominated by a nearby energy channel? Potentially, it would be more accurate to re-bin the HPCA flux into 16 energy channels instead of 63, and compare the >1 keV flux levels of these larger energy bins. Please discuss, currently it seems a bit misleading to describe the flux as being over such a narrow energy range.

Response: Thanks for the referee's nice comment and kind suggestion. The main purpose of calculating the O^+/H^+ particle fluxes ratio is to study the O^+ abundance at different energies on AE index and solar wind conditions (e.g. IMF By, IMF Bz and solar wind dynamic pressure) during the intense substorms. Since the energy range of O^+ and H^+ in the HPCA are the same. So we directly divide O^+ particle fluxes by H+ particle fluxes and we mainly focus on the ratios and not the values of their fluxes at specific energies.

Comments 10: Lines 231-236: Here it is stated that, "the maximum number density of energetic O+ at the dusk flank magnetopause is during the intense substorms recovery phase under the southward IMF. But the maximum ratio of n(O+)/n(H+) at the dusk flank magnetopause is during intense substorm recovery phase under the northward IMF. IMF Bz seems play a minor role in O+ abundance at the dusk flank magnetopause during intense substorm." It is not clear from the data as it is presented that this is true. The density ratio is of course dependent on O+ and H+ (which can come from the ionosphere and the solar wind). Comparing Figures 4a and 5a, it is not clear to me by eye that n(O+) is more dependent on By than Bz. It very well may be, but it is not readily apparent. Thus, is the density ratio difference actually from O+ or H+? Additionally, only 6 of the events in the study have a Bz > 0. This is notable, as Bz not being random does have an impact on the events. Thus, from this study it appears that Bz does play a role in the events being studied.

Response: Thanks for your valuable comments. Some descriptions determined by eye are not convincing. So I add the detailed information about density and corresponding IMF conditions in the supplement materials. The sentences in Line 231-136 have been revised by "The maximum density of energetic O^+ at the dusk flank magnetopause is under the southward IMF. Meanwhile, the maximum O^+/H^+ density ratio at the dusk flank magnetopause is under the southward IMF." The conclusion of "IMF Bz seems to play a minor role in O^+ abundance at the dusk flank magnetopause during intense substorm." In this manuscript is not rigid. So the relevant description has been removed. It noted that choosing the intense substorms one increase the probability of observing the southward IMF significantly. We found a nice

trend that O⁺ abundance increase with the IMF By. From Figure 6b, the O⁺/H⁺ density ratio show an obvious decrease with IMF Bz from -2 to 2 nT during the recovery phase (red crosses shown). Due to not enough statistical events (only 6 of the events in the study with northward IMF), some conclusions may be not convincing. As the MMS operating longer, more magnetopause crossing during intense substorm will be detected. It will be helpful. The relevant part "the IMF Bz seems play a minor role in O⁺ abundance at the dusk flank magnetopause during intense substorm." has been deleted.

Comments 11: Lines 241-242: "number density ratio at the dusk flank magnetopause during intense substorms have a weak correlation with the solar wind dynamic pressure." Can you quantify this correlation? In general, there are a lot of points currently that are driven from visual inspection of very scattered plots, when greater statistical rigor perhaps could be applied.

Response: Thanks for your suggestions. I agree with you, we need quantify this correlation and by eye is not rigid. So we fit the oxygen density dependence on pressure. Due to the number of events are limited (only 9 events during expansion phase) and distribution plot is very scattered, we don't think it makes sense to bin them according to some parameters. The sentence "number density ratio at the dusk flank magnetopause during intense substorms have a weak correlation with the solar wind dynamic pressure." has been removed. And substituted by more detailed description →"Figure 7a present that the O⁺ density at the dusk flank magnetopause during intense substorms has a positive correlation with the solar wind dynamic pressure. The empirical functional relation between the O⁺ density and solar wind dynamic pressure (from 1 to 4.5 nPa) is also established in the Eq.(3) and the corresponding correlation coefficient is 94%. From Figure 7b, the O⁺/H⁺ density ratio during recovery phase show a decrease from about 2.5 to 3 nPa. It is also noted that the O⁺/H⁺ density ratio increase with solar wind dynamic pressure from ~3 to 4 nPa."

Comments 12: Figures 4-7: The captions of the figures mention that the 95% confidence intervals are shown. Please mention this in the text and describe how it is calculated.

Response: Thanks for your kind suggestion. In the revised manuscript, we add the error bars in each point indicating a 90% Confidence Interval (CI). How to calculate the CI is described as follows: Step 1: find the number of observations n in the magnetopause boundary layer. Then calculate their mean $\bar{x}$ and standard deviation s. Step 2: Find the k value for 90% CI (the k value is 1.65). Step 3: use that k in this formula for the CI:

$$\bar{x} - k\frac{s}{\sqrt{n}} < \mu < \bar{x} + k\frac{s}{\sqrt{n}}$$

Where $\bar{x}$, s and n are the mean value, standard deviation and the sampling number of observations, respectively. k in the above formula can be determined by calculating a 90% CI for each events. See Line 286-292 in the "Tracked change" manuscript.

Very minor comments:

1. **Lines 103-106:** Please explicitly state that FPI does not discriminate between different ion species.

Response: thanks for your kind suggestion. We added the "FPI does not discriminate between different ion species" in the Line 136-137 in the "Tracked change" manuscript.

2. **Line 107:** Strictly speaking, HPCA measures up to 40 keV/q (thus for He^{++} this gets up towards 80 keV).

Response: Thanks for you carefully evaluate this manuscript. We agree with you, the HPCA maximum measurement for energy per charge is 40 keV/q. Line 138 in the "Tracked change" manuscript has been revised as you suggested.

3. **Line 116:** The authors might as well finish this thought, that this is due to spacecraft separation/scales of particle motion.

Response: Thanks for your nice suggestion. We added this sentence "this is due to spacecraft separation/scales of particle motion." into Line 150-151 in the "Tracked change" manuscript for finishing this thought.

4. **Line 296:** Fuselise et al. should be Fuselier.

Response: Thanks for you carefully evaluating this manuscript and giving important suggestions. We have revised this error. The other spelling and syntax errors have also been checked and corrected. See Line 430 in the "Tracked change" manuscript.

5. **Lines 304-306:** I would re-phrase this sentence. It is a minor distinction, but it currently reads as if you have studied energetic O+ across the entire magnetopause during substorms and found that the most prevalent region of O+ is the dusk flank during the recovery phase. Whereas, it should be more like, "Observations of energetic O+ at the dusk flank magnetopause during substorms are mainly found within the recovery phase."

Response: Thanks for referee's nice suggestion. We expand the statistical and found in our 57 events of energetic O^+ at the dusk flank magnetopause, there are 26 events during the expansion phase of intense substorms. While there are 31 events during the recovery phase of intense substorms. So this sentence is not meaningful and has been removed in the revised manuscript.

MMS observations of energetic oxygen ions at the ~~low-latitude~~ duskside magnetopause during intense substorms

Chen Zeng[1,2], Suping Duan[1], Chi Wang[1,2], Lei Dai[1], Stephen Fuselier[3,4], James Burch[3], Roy Torbert[5], Barbara Giles[6], Christopher Russell[7]

[1]State Key Laboratory of Space Weather, National Space Science Center, Chinese Academy of Sciences, China.

[2]University of Chinese Academy of Sciences, China.

[3]Southwest Research Institute, San Antonio, Texas, USA.

[4]The University of Texas at San Antonio, San Antonio, Texas, USA.

[5]University of New Hampshire, Space Science Center, Durham, New Hampshire, USA.

[6]NASA, Goddard Space Flight Center, Greenbelt, MD, USA.

[7]University of California Los Angeles, IGPP/EPSS, Los Angeles, California, USA.

Corresponding author: Chi Wang (cw@spaceweather.ac.cn), Suping Duan(spduan@nssc.ac.cn)

Abstract

Energetic oxygen ions ~~O^+~~ (~~>1keV~~ 1-40 keV) observed by the Magnetospheric Multiscale (MMS) satellites at the ~~dusk flank~~ duskside magnetopause boundary layer during ~~the~~ phase 1 ~~1a and 1b~~ are investigated. There are ~~31~~ 57 ~~dusk flank~~ duskside magnetopause crossing events during intense substorms (AE>500 nT) are identified. These ~~31~~ 57 events of energetic O^+ at the ~~dusk flank~~ duskside magnetopause include ~~9~~ 26 events during the expansion phase and ~~22~~ 31 events during the recovery phase of intense substorms. It is found that the O^+ density in the duskside magnetopause boundary layer during the recovery phase (0.081 cm^{-3}) is larger than that during the expansion phase (0.069 cm^{-3}). ~~It is noted that 9~~ The 26 events of energetic O^+ ion at the ~~dusk flank~~ duskside magnetopause during intense substorm~~s~~ expansion phase are all under the southward interplanetary magnetic field (IMF~~) conditions~~. There are only 7 events under northward IMF and they all occurred during the intense substorm recovery phase. The ~~number~~ density of energetic O^+ at the ~~dusk flank~~ duskside magnetopause ranges from ~~0.01~~ 0.007 ~~cm^{-3}~~ to ~~0.2~~ 0.599 cm^{-3}. The maximum ~~number~~ density ~~ratio~~ of O^+/H^+ ~~is ~0.055~~ occurred during the intense substorm recovery phase ~~and~~ ~~with AE index about 610 nT and~~ under ~~the nor~~ southward ~~interplanetary~~

31 ~~magnetic field (~~IMF~~)~~. When the IMF is southward, the O^+ density shows an exponential increase with

32 the IMF B_z absolute value. Meanwhile, The ~~number density ratio of~~ O^+/H^+ density ratio ~~also~~ shows an

33 exponential ~~increase~~ growth with the IMF B_y. These results agree with previous studies in the near-Earth

34 magnetosphere during intense substorm. It is suggested that O^+ abundance in the duskside magnetopause

35 boundary layer has a close relation with O^+ variations in the near-Earth magnetosphere during intense

36 substorms. ~~While IMF Bz seems play a minor role in O^+ abundance at the dusk flank magnetopause~~

37 ~~during intense substrom. Our observations suggest that energetic oxygen ions play a key role in the mass~~

38 ~~and energy transferring from the tail to the dayside in the magnetosphere during intense substorms.~~

1 Introduction

40 Single charged oxygen ions (O$^+$) in the magnetosphere, ~~O^+,~~ are exclusively from the ionosphere.

41 They are an important element in the mass and energy transport in the magnetospheric dynamic process

42 ~~during intense substorms (AE >500 nT)~~, especially during the expansion phase and recovery phase of

43 intense substorms (e.g., Daglis et al., 1991~~;~~, 1996; Duan et al., 2017; Fok et al., 2006; Ohtani et al., 2011;

44 Ono et al., 2009; Nosé et al., 2000; Yau et al.,1997~~;~~, 2012; Kronberg et al., 2014). Processes in the

45 magnetotail due to substorm can result in auroral electrojet activity. This activity is generally caused by

46 field-aligned currents increase and reflected by the AE index (Tang and Wang, 2018). Previous studies

47 have found that ~~T~~the ~~number~~ density and energy density of ~~oxygen ions,~~ O^+, significantly increase with

48 AE index in the near-Earth magnetosphere during the intense substorm ~~expansion phase~~ (e.g.,

49 Lennartsson and Shelley, 1986; Daglis et al., 1991, 1994; Duan et al., 2017~~; Lennartsson and Shelley,~~

50 ~~1986~~). Lennartsson and Shelley (1986) proposed that oxygen ions with energies less than 17 keV/e could

51 provide 50% of the density in the plasma sheet during disturbed geomagnetic activity. They found the

52 increase in the O^+ energy density was strongest around local midnight where O^+ became the most

53 abundant ion at AE~1000 nT. In the near-Earth plasma sheet (NEPS), The O^+ energy density has an

54 explosively increases with AE index in the range of larger than 500 nT during the intense substorm

55 expansion phase (Daglis et al., 1994). Previous studies reported that the O^+ from the nightside auroral

56 region could rapidly feed in the near-Earth magnetosphere during substorm expansion phase (e.g., Daglis

57 and Axford, 1996; Duan et al., 2017; Yu et al., 2013). Otherwise, the solar wind dynamic pressure also

58 influences the oxygen content of ion outflow from the ionosphere. Using the Thermal Ion Dynamics

59 Experiment (TIDE) on the Polar satellite. Elliott et al., (2001) found both the O^+ density and parallel flux

60 increased with the solar wind dynamic pressure.

61   The O^+ outflowing from the ionosphere with low energy of eV are accelerated to about 500 eV at

62 the high altitude polar region (e. g., Yau and André, 1997). Then they are convected tailward into the

63 lobe and the plasma sheet boundary layer. After O^+ enter the NEPS of magnetotail, they can be energized

64 up to tens of keV during intense substorm dipolarizations（e.g., Birn et al., 2013; Duan et al., 2017;

65 Fok,et al., 2006; Nosé et al., 2000; Ono et al., 2009; Yau et al., 2012). ~~Daglis et al. (1991) reported that~~

66 ~~the energy density of O^+ increased non-linearly with AE indices during substorms.~~ The inductive electric

67 field associated with substorm dipolarization is very significant for accelerating particles in the ~~near-~~

68 ~~Earth plasma sheet~~NEPS (e.g., Dai et al.,~~,~~ 2014~~;~~, 2015; Duan et al.,~~,~~ 2011,~~ ;~~2016; Lui et al.,~~,~~ 1999).

69 ~~Lennartsson and Shelley (1986) proposed that oxygen ions with energy of less than 17 keV/e can provide~~

70 ~~50% of the number density in the plasma sheet during activity geomagnetic disturbance.~~ Duan et al.

71 (2017) reported that the O^+ from the lobe or the plasma sheet boundary layer were efficiently accelerated

72 by the kinetic Alfven eigenmode with significant unipolar electric field and rapidly feed in the NEPS

73 during intense substorm dipolarizations. These energetic O^+ in the NEPS can be injected into the inner

74 magnetosphere and drift westward into the duskside outer magnetosphere (e.g., Ganushkina et al., 2005).

75 ~~The oxygen ions from the nightside auroral region can rapidly feed in the near Earth magnetosphere~~

76 ~~during substorm expansion phase (e.g., Daglis and Axford, 1996; Duan et al., 2017; Yu et al., 2013).~~

77   Oxygen ions decay from the ring current ~~and~~ can leak~~ed~~ into the dayside ~~low latitude~~magnetopause

78 boundary layer (e.g., Li et al., 1993; Ebihara et al., 2011). Li et al. (1993) reported that the ring current

79 O^+ with tens of keV energy interacted with the Pc 5 waves and then lost towards the dayside

80 magnetopause. ~~Kim et al. (2005) pointed out that~~ The solar wind dynamic pressure enhancement plays~~ed~~

81 a key role in the ~~loss of the~~ ring current particle loss into the outer magnetosphere. This pressure

82 enhancement pushing the magnetopause to move inward leads to a reduction of the scale length of the

83 magnetic field magnitude gradient along the magnetopause. The magnetic gradient drift speed across the

84 magnetopause will increase. So the ring current oxygen ions along the magnetic gradient drift path can

85 easily enter into the outer magnetosphere (Kim et al., 2005). Ebihara et al. (2011) proposed that the field

86 line curvature scattering ~~is~~ was more effective on the loss of energetic oxygen ions with its large gyro-

87 radius. The~~se~~ energetic oxygen ions with pitch angle of ~90 degrees ~~can~~ are more prone to leak into the

88 dayside magnetopause. ~~This process may be the key loss mechanism for the ring current ions.~~

89   The <u>distribution of</u> energetic oxygen ions density at the dayside magnetopause is asymmetry

90   ~~distribution~~ and <u>it</u> has <u>a</u> close relationship with the interplanetary magnetic field <u>(IMF)</u> ~~and solar wind~~

91   ~~dynamic pressure~~ (e.g., Bouhram et al., 2005; Phan et al., 2004<u>; Luo et al., 2017</u>). Bouhram et al. (2005)

92   pointed out that the O^+ density <u>in the duskside (on average 0.053 cm^{-3}) magnetopause</u> is higher ~~in the~~

93   ~~duskside~~ than <u>that</u> in the dawn–side <u>(on average 0.014 cm^{-3})</u> ~~magnetopause~~. <u>They found</u> O^+ ~~is~~ <u>was</u> the

94   dominant contributor to the mass density <u>(</u>30%<u>)</u> on the dusk-side <u>magnetopause</u> in comparison to 3% in

95   the dawnside and 4% near <u>the</u> noon. <u>The dawn-dusk asymmetries of the energetic O^+ (>~274 keV)</u>

96   <u>distribution in three different regions (dayside magnetopause, near-Earth nightside plasma sheet, and tail</u>

97   <u>plasma sheet) are also observed by Luo et al., (2017). They found that the energetic O^+ distributions were</u>

98   <u>mainly influenced by the dawn-dusk IMF directions and the enhancement of ion intensity strongly related</u>

99   <u>to the location of the magnetopause reconnection.</u> ~~Phan et al. (2004) reported that energetic O^+ with~~

100   ~~energy larger than 3 keV in the reconnection jets are observed by Cluster at the duskside mid-latitude~~

101   ~~magnetopause under steady southward interplanetary magnetic field (IMF) conditions.~~

102   There is ample evidence that magnetospheric ions could participate in the magnetopause

103   reconnection and directly escape along <u>the</u> reconnected open field lines (e.g., Sonnerrup et al.,1981;

104   Fuselier et al., 1991,<u>2016</u>; Slapak et al., 2012,<u>2015</u>; Wang et al., 2014; Liu et al., 2015). <u>The energetic</u>

105   <u>O^+ with energies larger than 3 keV in the reconnection jets at the duskside mid-latitude magnetopause</u>

106   <u>under steady southward IMF was reported by Phan et al. (2004).</u> ~~(~~Zong et al., (2001) observed O^+

107   energy dispersion due to time-of-flight (TOF) effects at the ~~dusk flank~~<u>duskside</u> magnetopause under

108   southward IMF and it was assumed that O^+ was escaping from the ring current along the reconnected

109   field lines during steady reconnection. However,~~However~~, Fuselier et al. (1989) reported <u>that</u> O^+ from

110   the high latitude ionosphere <u>were</u> not associated with any substorm cycle. O^+ from the high latitude

111   ionosphere could form the O^+ rich boundary layer in the low latitude magnetopause. ~~While~~<u>When</u> O^+ enter

112   <u>the reconnection jets,</u> the reconnection rate is likely reduced by the mass-loading ~~, reconnection is~~<u>but</u> not

113   suppressed at the magnetopause <u>(</u>~~-~~Fuselier et al. 2019).

114   At present, <u>variations of</u> O^+ <u>abundance (O^+/H^+) in the duskside magnetopause boundary layer</u>~~near~~

115   ~~the dayside low-latitude magnetopause~~ during <u>intense</u> substorm <u>(AE >500 nT) on AE index and solar</u>

116   <u>wind conditions (e.g. IMF B_y, IMF B_z and solar wind dynamic pressure)</u> ~~expansion phase and recovery~~

117   ~~phase~~ are still not ~~understood~~<u>clear</u>. Previous studies of <u>O^+ abundance variations</u>~~oxygen ions~~ during

118   substorms are mainly focused on ~~O^+ energizations in the near Earth plasma sheet in~~ the magnetotail <u>or</u>

119 the near-Earth region (e.g., Duan et al., 2017; Nosée et al., 2000; Ohtani et al., 2011). The

120 Magnetospheric Multiscale (MMS) mission gives us an opportunity to focus on the O⁺ in the duskside

121 magnetopause region. In this study, ~~W~~we investigate statistical features of energetic ~~oxygen ions~~O⁺ at

122 the ~~dusk flank~~duskside magnetopause and their relations with AE index and solar wind conditions (e.g.

123 IMF B_y, IMF B_z, and solar wind dynamic pressure)~~O+ in the near-Earth plasma sheet~~ during the intense

124 substorms (AE >500 nT).

125 **2 Instrumentation and Data**

126 ~~Instrumentation and data~~

127 ~~2.1 Instrumentation and data~~

128   This study ~~uses~~ used data from the Magnetospheric Multiscale (MMS) mission. This mission

129 comprises four identical satellites that were launched on 2015 March 13 into an elliptical 28-inclination

130 orbit with perigee around 1.2 R_E and apogee around 12 R_E (Burch et al., 2016; Fuselier, et al., 2016b).

131 The electric field **E** is from the electric double probe (EDP) (Ergun et al., 2016; Lindqvist et al., 2016),

132 and magnetic field **B** is from the Fluxgate Magnetometer (FGM) (Russell et al., 2016). The plasma data

133 are from the Fast Plasma Investigation (FPI) (*Pollock et al., 2016*) and the Hot Plasma Composition

134 Analyzer (HPCA) (*Young et al., 2016*). The FPI provides plasma (electrons and ions) distribution

135 functions at 32 energies from 10 eV to 30 keV. And it has a high time resolution of 0.03 s for electrons

136 and 0.15 s for ions in the burst mode and 4.5 s in the fast mode (Pollock et al., 2016). The FPI does not

137 discriminate between different ion species. While ~~T~~the HPCA provides ion composition (H⁺, He⁺⁺, He⁺,

138 and O⁺) measurements in the energy range from ~1 eV/q to 40 keV/q (Young et al., 2016). Although the

139 HPCA instrument employs radio frequency (RF) unit to artificially reduce the proton fluxes in some

140 areas where the proton fluxes are intense, there still exists a low level of background that affects the O⁺

141 fluxes in the magnetosheath. The majority of the O⁺ fluxes in the magnetosphere side of the

142 magnetopause are at energies ~~above~~ from 1 keV to 40 keV and that band below 1keV visible in the

143 magnetosheath side are observations outside the RF operating range and contamination from high proton

144 fluxes. Due to this contamination, the ~~number~~ O⁺ ~~density of O⁺ with~~at energ~~y~~ies from ~~above~~ 1 keV to

145 40 keV ~~is~~ in the magnetopause boundary layer are considered ~~at the magnetopause~~ in our study. The O⁺

density recalculated from the HPCA distribution functions at this energy range by using the Space Physics Environment Data Analysis System (SPEDAS) software package. More details about SPEDAS can be found in Angelopoulos et al. (2019). The solar wind parameters, ~~IMF~~ and AE index are available from the OMNI data in CDAweb (http://cdaweb.gsfc.nasa.gov/). The data from the MMS 4 satellite are adopted in our investigation since the data difference from other three spacecraft is negligible. This is due to spacecraft separation and scales of particle motion.

~~2.2 Energetic O+ at the dusk flank magnetopause during intense substorms~~

~~2.2.1~~ 3 Results

3.1 Detailed event on 3 October 2015

Figure 1 presents the three components of the IMF in Geocentric Solar Magnetospheric (GSM) coordinates, solar wind dynamic pressure ~~and~~, as well as AU, AL, and AE index during the ~~interval~~ time of interest from 14:30 ~~UT~~ to 16:30 UT on 3 October 2015. During this interval, the IMF B_x component is negative all the time (Figure 1a). Its maximum value is about -1 nT at ~15:16 UT. The IMF B_y component is almost negative except at ~14:32 and ~16:23 UT. The negative IMF B_z component is also observed ~~negative~~ during this interval as shown in Figure 1c. The minimum value of the IMF B_z component is about ~~-6.7~~7.1 nT at ~14:30 UT. The solar wind dynamic pressure is only at the beginning of the time interval about 2 nPa. Then, it increases sharply at 15:~~10~~00 UT and reaches its maximum value about 4.4 nPa at ~15:12 UT. ~~The maximum solar wind dynamic pressure is about 4 nPa. An intense substorm (AE > 500 nT) occurred under the above IMF and solar wind dynamic pressure. The substorm onset time is about 14:45 UT, when the AE index significantly increases. The maximum value of AE index is ~1000 nT at 15:20 UT.~~ These solar wind conditions led to an intense substorm (AE > 500 nT), as Figure 1g shown. The AE index is defined as AE=AU-AL. Generally, the substorm onset time is characterized by the AL index starting to significantly decrease and the AE index significantly increase. The interval of the AL index decreasing from onset to its minimum is defined as the substorm expansion phase. The interval of the AL index increasing from the minimum to the quiet time level is regarded as the substorm recovery phase. From Figure 1e to 1g, the substorm onset time is about 14:45 UT marked by the AL index starting to sharply decrease and AE index increasing. After the AE index significantly increases and the AL index decreases (Figure 1f), the AL and AE indexes reach their minimum and

174   maximum values about -750 nT and 1000 nT at ~15:20 UT, respectively. This interval from ~14:45 to

175   ~15:20 UT is regarded as the intense substorm expansion phase. Then, the intense substorm enters the

176   recovery phase as the AL index gradually increases and AE index decreases after ~15:20 UT. The two

177   blue dashed lines indicate the time interval of the magnetopause boundary layer crossing. According to

178   the above description, we can identify this magnetopause boundary layer crossing occurred during the

179   recovery phase of intense substorm. The identification of the magnetopause boundary layer will be

180   described later.

181   Figure 2 shows ~~that MMS 4 encountered the duskside magnetopause region~~ the overview of the

182   magnetopause inbound crossing from ~~15:25:10~~15:00 to ~~15:36:50~~16:00 UT ~~during the intense substorm~~

183   ~~recovery phase~~ on 03 October 2015. ~~This interval is marked by the two vertical blue lines in Figure 1.~~

184   ~~This intense substorm onset time is around 14:45 UT with AE maximum value 1000 nT at 15:20 UT as~~

185   ~~shown in Figure 1e.~~ During the magnetopause crossing, MMS 4 satellite~~s were~~ was located at about ~~(~~(6.0,

186   8.8, -5.1~~)~~) ~~Re~~ R_E in GSM as shown in the bottom of Figure 2. From top to bottom, panels 2a and 2b show

187   ~~that~~ the magnetic and electric fields in GSM from FGM and EDP, respectively. Ion and electron

188   temperature~~s,~~ ~~ion and electron~~ plasma density ~~number densities,~~ and ion velocity in GSM from FPI L2

189   data products are shown in Figure~~s~~ ~~2c, 2d and 2e~~2c-e, ~~respectively.~~ Figure 2f shows the H^+ and O^+

190   densities, followed by ~~Tt~~he electron and ion omnidirectional differential energy fluxes~~omnidirectional~~

191   ~~electron and ion energy fluxes~~ from FPI ~~are shown in~~ (Figure 2g~~-h and 2h~~). ~~, respectively. The O+ number~~

192   ~~density at energies above 1keV is displayed in Figure 1f.~~ The last four panels ~~of Figure 2 show~~ present

193   the ~~omnidirectional~~ differential fluxes of four individual ion species, H^+, O^+, He^+ and He^{++} measured by

194   HPCA, respectively. The HPCA flux in panels 2i-l has artificial striping every 4 energy bins due to way

195   HPCA determines the count rate over 4 energy channels in survey mode. It is noted that the differential

196   fluxes (Figure 2i-l) and differential energy fluxes (Figures 2g-h) have different units. To better identify

197   the fluxes variations at specific energies, we choose the ion and electron fluxes from FPI in the energy

198   flux unit. The plasma moments (e.g. ion parallel and perpendicular temperatures, ion and electron

199   densities, and ion velocity) from FPI shown in Figures 2c-e are all from MMS L2 data products. They

200   are default moments calculated over the full FPI energy range from 10 eV to 30 keV. Note that in the

201   magnetosheath, O^+ measurements suffer from fake counts at energies below 1 keV which results from

202   high proton fluxes contamination, as the red box in Figure 2j shown. So the spurious counts should be

203   excluded in the plasma moments calculation. The O^+ density shown in Figure 2f is recalculated from

204 HPCA distribution functions at energies from 1 keV to 40 keV. Due to H^+ measurements from HPCA is

205 accurate and the H^+ mean energy in the magnetosheath is typically 0.3 keV, we adopted the default H^+

206 density from HPCA L2 data products which computed over the full HPCA energy range from 1 eV to

207 40 keV, as the red line shown in Figure 2f.

208   The different regions encountered by MMS4 during the interval of 15:00 to 16:00 UT are marked

209 by the colored bar at the top of Figure 2, with the magnetosheath shown in orange, the outer

210 magnetosphere shown in blue, and the magnetopause ~~region~~ boundary layer shown in green. From

211 15:00:00 to 15:25:10 UT, MMS4 was located in the magnetosheath. This region is characterized by ~~a~~ the

212 southward magnetic field, low ion and electron temperatures (~~a few hundred~~ a few hundred eV for ions

213 and tens of eV for electrons, Figure 2c) with relatively high ~~number~~ densities (on the order of ~20 cm^{-3},

214 Figure 2d), and stable ion flow speed~~s~~ of about ~~one hundred~~ 100 km/s. There are also very high fluxes at

215 energies centered around 100 eV (nominal magnetosheath energy) for electrons (Figure 2g) and at

216 energies centered around 1 keV ~~–~~ for ions (Figure 2h, also see H^+ fluxes in Figure 2i and He^{++} fluxes in

217 Figure 2l) in the magnetosheath. While the O^+~~He$^+$~~ and ~~O$^+$~~ He^+ fluxes above 1 keV nearly disappear in

218 the magnetosheath (Figure 2j and 2k). From Figure ~~2k~~ 2j, the majority of the ~~–~~ O^+ fluxes at energies below

219 1 keV visible in the magnetosheath are the result of contamination from the high proton fluxes, as the

220 red box indicated.

221   The primary magnetopause crossing from the magnetosheath into the magnetosphere last~~ed~~ed about

222 ~~6~~ 12 min, from ~~15:31:20~~ about 15:25:10 to 15:36:50 UT. Partial encounters of the magnetopause by

223 MMS4 occurred around 15:43:15, 15:47:10 ~~and~~, 15:53:00 UT and etc.~~, respectively.~~ The magnetopause

224 ~~region~~ boundary layer is identified by the plasma moments~~particle fluxes~~ and the electromagnetic field.

225 The plasma density and ~~ion~~ temperature at the magnetopause are between the corresponding values of

226 the magnetosphere and the magnetosheath, as shown in Figure 2d and 2c~~, respectively~~. The

227 magnetopause ~~region~~ boundary layer can also be identified by the significant increases in electron fluxes

228 at energies about several hundred~~s of~~ eV and ion fluxes at energies around ~10 keV, as shown in Figure

229 2g and 2h, respectively. During ~~the interval from 15:25:10 to 15:36:50U~~t this time of interest, the B_z

230 component rotated from southward to northward and back again several times before finally became

231 northward when MMS 4 entered the magnetosphere. The energetic O^+ ~~number~~ density (1-40 keV) is

232 around 0.~~02~~018 cm^{-3} within the magnetopause boundary layer as shown in Figure 2f. The corresponding

233 H^+ and O^+ fluxes at specific energies and their densities (shown in Figure 2f) were averaged in this region.

234   After 15:36:50 UT, MMS4 entered the magnetosphere which is identified by the observations of ~~a~~

235 the northward magnetic field (Figure 2a), much lower ~~number~~ plasma densities (on the order of ~1 cm$^-$

236 ^{3}) with respect to the densities in the magnetosheath (Figure 2d), higher ~~ion~~ plasma temperatures (~~(~~Figure

237 2c, several~~a few thousands of~~ keV for ions and a few hundred eV for electrons), and a small bulk ion

238 flow speed. Higher fluxes at energies~~–~~ around several keV for electrons (Figure 2g) and at energies

239 centered around ~10 keV for ions (Figure 2h) also indicate that the MMS4 was in the magnetosphere.

240 Finally, the presence of O^+ ~~He$^+$~~ and ~~O^+~~ He^+ at energies about ~10 keV is also used as a marker to verify

241 that MMS4 was in the magnetosphere (Figure 2j and 2k).

242 **~~2.2.2~~ 3.2 Statistical ~~3~~157 events of ~~MMS first Phase 1 observations of~~ energetic O^+ at the ~~dusk~~**

243 **~~flank~~duskside magnetopause ~~crossing~~ during intense substorms~~(AE>500nT)~~**

244   Based on the in-situ measurements of the dayside magnetopause ~~processes~~ crossings by MMS

245 satellites in phase 1~~a and phase 1b~~, we identified the duskside magnetopause crossing event (complete

246 magnetopause crossing from the magnetosheath to the magnetosphere, vice versa) from the summary

247 plot in https://lasp.colorado.edu/mms/sdc/public/plots/. Then we plotted the more detailed overview

248 figure of these events to identify the magnetopause boundary layer, as Figure 2 shown. Only events with

249 AE index larger than 500 nT during the magnetopause boundary layer crossings interval were selected.

250 There are ~~31~~ 57 events of the ~~dusk flank~~dusksideside magnetopause boundary layer crossing during

251 intense substorm ~~during intense substorms with AE index larger than 500 nT~~satisfied with the above

252 criterion ~~are selected~~. In our statistical study, the mean values of the H^+ and O^+ fluxes at specific energies

253 and their densities are calculated in the magnetopause boundary layer. Correspondingly, the solar wind

254 dynamic pressure~~and~~, IMF ~~B_z~~B_y, B_{yz} and AE index from the OMNI data system ~~was~~ were averaged

255 during the magnetopause boundary layer crossing time interval, as the two blue dashed lines shown in

256 Figure 1. The phase of the substorm is determined from the variations of AU, AL and AE index~~es~~, as

257 mentioned before. For better follow-on studies, we add more detail information about 57 energetic O^+

258 events into an appendix. From the appendix, we can easily draw the conclusion that the O^+ density in the

259 duskside magnetopause during the recovery phase (0.081 cm^{-3}) of intense substorm is larger than that

260 during the expansion phase (0.069 cm^{-3}).

261   Figure 3 displays the locations of 57 energetic O^+ events at the duskside magnetopause (-5.7 $R_E <$

262 $Z_{GSM} < 1.7 R_E$) during intense substorms projected into the XY_{GSM} plane ~~of 31 events of energetic O^+ at~~

263   ~~the dusk flank magnetopause during intense substorms~~. The blue curve line represents the nominal

264   magnetopause, which is obtained by the magnetopause model of ~~(~~Shue et al., (1998)~~)~~ ~~using~~when the IMF

265   B_z is about ~ ~~-1.96~~ 3.21 nT and solar wind dynamic pressure (Psw) is ~ ~~2.37~~2.87 nPa (averaged for the

266   ~~31~~ 57 events). The diamond and circle represent the event at the ~~dusk flank~~duskside magnetopause during

267   the intense substorm expansion phase and recovery phase, respectively. The O^+ ~~number~~ density and the

268   ~~number density ratios of~~ O^+/H^+ density ratio are shown by the colored diamonds and circles at the

269   corresponding magnetopause locations in Figures 3a and 3b, respectively. Among the ~~31~~ 57 events of

270   energetic O^+ at the ~~dusk flank~~duskside magnetopause during intense substorms, there are ~~9~~26 events that

271   occurred during the expansion phase of intense substorms and ~~22~~31 events ~~occurring~~ occurred during

272   the recovery phase ~~of intense substorms. These 9 and 22 events are shown in Figure 3 by 9 diamonds~~

273   ~~and 22 circles, respectively.~~ The maximum ~~number~~ density of energetic O^+ is found during the intense

274   substorm recovery phase as presented in Figure 3a. ~~On the other hand, the maximum number density~~

275   ~~ratio of O+/H+ is also found during the recovery phase of an intense substorm as shown by the red circle~~

276   ~~in Figure 3b.~~

277   Figure 4 presents the relationship between the energetic O^+ at the ~~dusk flank~~duskside magnetopause

278   and AE index during intense substorms. From top to bottom, panels show ~~that~~ the O^+ and H^+ ~~number~~

279   ~~density~~densities (Figure 4a), the O^+/H^+ ~~number~~ density ratio ~~of O+/H+,~~ (Figure 4b)~~,~~ and O^+/H^+ particle

280   fluxes ratios at different energy ranges ~~of O+/H+~~ (Figure 4c), respectively. The energy channel ranges

281   ~~of~~for O^+ and H^+ in the HPCA are the same. So the ~~O+/H+ number density ratio (nO+ / nH+) and~~ O^+/H^+

282   particle fluxes ratio are directly defined as the ratio between mean values of their fluxes, respectively.

283   ~~for~~ The particle fluxes are chosen~~(fO+ /fH+)~~ at energies ~1 keV (energy range from 987.82 to 1165.21

284   eV), ~10 keV (energy range from 99.73~~.98~~ to 11.77~~65.13~~ keV), ~20 keV (energy range from 19.31~~0.05~~

285   to 22.77~~7.82~~ keV) and ~35 keV(energy range from 31.69~~3.41~~ to 37.39~~85.04~~ keV). ~~are defined as the~~

286   ~~ratio between mean values of their number densities and fluxes, respectively.~~ The error bars indicating

287   the 90% confidence interval (CI) are also overplotted in each point. The confidence interval is based on

288   the following formula:

289 $$\bar{x} - k\frac{s}{\sqrt{n}} < \mu < \bar{x} + k\frac{s}{\sqrt{n}}$$

290   Where $\bar{x}$, s and n are the mean value, standard deviation and the sampling number of observations,

291   respectively. k in the above formula can be determined by calculating a 90% confidence interval for each

292 events (the k value is 1.65). Figure 4a shows that ~~the number density of~~ energetic O$^+$ density at the ~~dusk~~

293 ~~flank~~duskside magnetopause during intense substorms is in the range from ~~0.01~~ 0.007 ~~cm^{-3}~~ to ~~0.2~~0.599

294 cm^{-3}. The maximum ~~number~~ density value of energetic O$^+$ at the ~~dusk flank~~duskside magnetopause

295 during intense substorm ~~expansion~~ recovery phase is presented at the higher AE index ~~about 870~~ 606

296 nT ~~as displayed in Figure 4a the last right blue circle. While the maximum value of the energetic O+~~

297 ~~number density, the ratio of nO+ / nH+, and fO+ /fH+ at the dusk flank magnetopause during intense~~

298 ~~substorm recovery phase are all around AE index 600 nT.~~ The O$^+$/H$^+$ density ratio decreases with AE

299 index from 900 to 1100 nT. The variations of O$^+$ density and O$^+$/H$^+$ density ratio with AE index do not

300 show obvious difference between during the expansion phase and the recovery phase.

301   Figure 5 shows the relationship between the energetic O$^+$ at the ~~dusk flank~~duskside magnetopause

302 and ~~the~~ IMF B$_y$ during intense substorms. The format of ~~the~~ Figure 5 is the same as that of Figure 4.

303 Figure 5a shows that the O$^+$ and H$^+$ ~~number~~ densities ~~increase~~ decrease with IMF B$_y$ ~~when it is larger~~

304 ~~than 4 nT~~ from -6 to 0 nT and increase with IMF B$_y$ from 4 to 8 nT. From Figure 5b, the O$^+$/H$^+$ ~~number~~

305 density ratio shows an exponential growth with ~~increase in~~ the IMF B$_y$ ~~is associated with an exponential~~

306 ~~growth by a factor 0.07~~. Based on ~~observations~~ the scatter plot in Figure 5b, we can define linear

307 functional dependence between the logarithm of O$^+$/H$^+$ ~~number~~ density ratio and IMF B$_y$, as Eq. (1)

308 ~~shown.;~~ And the corresponding correlation coefficients is 94%. The correlation coefficient close to 100%

309 indicates that there is a great correlation.

310   ~~$\log(n^{O\pm}/_{H\pm}) = 0.07 * \text{IMF By} - 5.14$~~   (1)

311      $$\log \frac{n_{O^+}}{n_{H^+}} = 0.126 * \text{IMF By} - 5.174$$ (1)

312   The dependency is constructed using a linear ~~least~~ least-squares fit unless otherwise stated. The

313 O$^+$/H$^+$ particle flux ratio at energy ~~about~~ ~10 keV, ~20 keV and ~~~30~~35 keV also show an obvious

314 exponential increase with IMF B$_y$. This dependency is consistent with Welling et al. (2011) simulation

315 results found in the ring current.

316   Figure 6 shows the relationship between the energetic O$^+$ at the ~~dusk flank~~duskside magnetopause

317 and ~~the~~ IMF B$_z$ during intense substorms. The format of ~~the~~ Figure 6 is the same as that of Figure 4.

318 Figure 6a and ~~Figure~~ 6b both present that among ~~our 31~~ 57 events of energetic O$^+$ ~~near~~ at the ~~dusk~~

319 ~~flank~~duskside magnetopause boundary layer during intense substorm, there are 50 events under

320 southward IMF and only 7 events under northward IMF.~~there are 9~~ It is noted that 26 events occurred

321 during the expansion phase of intense substorms which are all under the southward IMF conditions, as

322 the blue points shown ~~the blue circle in Figure 6~~. ~~While~~ Meanwhile, the~~re are only 6~~ events that

323 occurred under ~~the~~ northward IMF are all during the intense substorm recovery phase, as the right ~~circle~~

324 red points with positive IMF B$_z$ ~~> 0~~ shown. From -10 to 0 nT, the O$^+$ density shows an obvious decrease

325 with IMF B$_z$. To better describe this variation trend, the empirical functional relation between the

326 logarithm of O$^+$ density and IMF B$_z$ (from -10 to 0 nT) is established in Eq.(2) and the corresponding

327 correlation coefficient is 94%. While the O$^+$ density has a positive correlation with IMF B$_z$ from 0 to 5

328 nT.

329
$$\log n_{O^+} = -0.163 * \text{IMF Bz} - 3.737 \qquad (2)$$

330 From Figure 6b, the O$^+$/H$^+$ density ratio during the recovery phase decrease with IMF B$_z$ from about -2

331 to 2 nT. The maximum ~~number~~ density of energetic O$^+$ at the ~~dusk flank~~ duskside magnetopause is ~~during~~

332 ~~the intense substorms recovery phase~~ under ~~the~~ southward IMF. ~~But~~ Meanwhile, the maximum O$^+$/H$^+$

333 density ratio ~~of nO+ / nH+~~ at the ~~dusk flank~~ duskside magnetopause is also ~~during intense substorm~~

334 ~~recovery phase~~ under ~~the northward~~ southward IMF. ~~Comparing with IMF By, IMF Bz seems play a~~

335 ~~minor role in O+ abundance at the dusk flank magnetopause during intense substrom.~~

336 Figure 7 displays the relationship between the energetic O$^+$ at the ~~dusk flank~~ duskside magnetopause

337 and ~~the~~ solar wind dynamic pressure during intense substorms. The format of ~~the~~ Figure 7 is the same as

338 that of Figure 4. Figure 7a ~~and 7b both~~ presents that the ~~number~~ O$^+$ density ~~of energetic O+ and the O+~~

339 ~~to H+ number density ratio~~ at the ~~dusk flank~~ duskside magnetopause during intense substorms ~~have~~ has a

340 ~~a weak~~ positive correlation with the solar wind dynamic pressure. The empirical functional relation

341 between the logarithm of O$^+$ density and solar wind dynamic pressure (from 1 to 4.5 nPa) is also

342 established in Eq.(3) and the corresponding correlation coefficient is 94%.

343
$$\log n_{O^+} = 0.325 * \text{Psw} - 4.061 \qquad (3)$$

344 From Figure 7b, the O$^+$/H$^+$ density ratio during recovery phase show a decrease from about 2.5 to 3 nPa.

345 It is noted that the O$^+$/H$^+$ density ratio increase with solar wind dynamic pressure from about 3 to 4 nPa.

346 The maximum ~~number~~ density of energetic O$^+$ at the ~~dusk flank~~ duskside magnetopause, ~~~ 0.2~~ ~0.599

347 cm^{-3} take place at solar wind dynamic pressure ~~is 1.9~~ about 3.9 nPa ~~during an intense substorm recovery~~

348 ~~phase~~. While the maximum O$^+$ ~~to~~ /H$^+$ ~~number~~ density ratio at the ~~dusk flank~~ duskside magnetopause ~~is~~

349 ~~around~~ appeared at solar wind dynamic pressure ~~around 2.5~~ 2.2 nPa. More details can be found in the

350 appendix.

351

~~4~~3 Discussion

Energetic O^+ (1-40 keV) with high ~~number~~ density are observed by ~~the~~ MMS satellites at the ~~dusk flank~~duskside magnetopause during the expansion phases and recovery phases of intense substorms, as displayed in Figure 3a ~~and Figure 4a~~. The ~~number~~ density of energetic ~~oxygen ions~~O^+ is in range from ~~0.01~~0.007 cm^{-3} to 0.~~25~~99 cm^{-3} at the duskside ~~flank~~ magnetopause boundary layer during intense substorms. ~~This O+ number density is larger than the energetic O+ near the duskside mid latitude magnetopause observed by Cluster, which was 0.011 to 0.053 cm 3 (e.g., Bouhram et al., 2005). Bouhram et al. (2005) demonstrated that the O+ number density is much higher in the dusk side than in the dawn side magnetopause.~~ In a companion paper from Zeng et al. (2019), they study the O^+ abundance variations on the solar wind conditions at the dayside magnetopause boundary layer and not specific to the events that occurred during intense substorm. The mean value of the O^+ density at the duskside magnetopause boundary layer is 0.038 cm^{-3} in that paper. While during the intense substorm, the O^+ density increase to 0.075 cm^{-3} in this study. ~~The significantly higher number density of energetic O+ is obtained from MMS at the dusk flank magnetopause during intense substorms in our paper.~~ There are two reasons for this high ~~number~~ density of energetic O^+ observed during the intense substorm. The first is the time interval for the observations. Our observations are during intense substorms expansion phase and recovery phase. Daglis et al. (1991) proposed that energetic O^+ were significantly higher in the ~~near Earth plasma sheet~~NEPS in the magnetotail after intense substorms onset. The impulsive electric field accompanied by intense substorm dipolarization plays a key role in the energization and sunward transfer of oxygen ions in the duskside of midnight plasma sheet in the magnetotail (e.g., Fok et al., 2006; Nos~~e~~é et al., 2000). These energetic O^+ (tens of keV) can be transported sunward into the ~~low latitude~~duskside magnetopause boundary layer. The second reason for the high densities is the locations of the observations. Our observations are near the ~~dusk flank~~duskside magnetopause. This region is easily accessible by energetic O^+ during intense geomagnetic activity (Fuselier et al. 2016a). Phan et al. (2004) pointed out that energetic O^+ ~~were observed~~ with very high ~~number~~ density 0.2-0.3 cm^{-3} in the reconnection jets at the dusk~~-~~side mid-latitude magnetopause were observed by Cluster.

378 During dynamic periods and intense substorms time, light ions yielded more symmetric patterns in

379 density than heavy ions and the O^+ patterns in the active plasma sheet are a function of IMF conditions

380 (Winglee and Harnett 2011. Winglee et al. 2005). Welling et al. (2011) used multispecies MHD and the

381 PWOM to drive a ring current model, and found that positive IMF B_y ~~pushing~~ pushed the stronger O^+

382 concentrations toward the duskside at a geocentric distance of about 6.6 R_E. This O^+ density duskward

383 preference with positive IMF B_y in the ~~near Earth plasma sheet~~NEPS is similar to our results. It may

384 indicate that ~~the~~ O^+ in the ~~dusk flank magenetopause~~ magnetopause boundary layer ~~O^+~~-enhancing with

385 IMF B_y is due to the local time variations of O^+ in the ~~near Earth plasma sheet~~NEPS tied to IMF B_y.

386 ~~While IMF Bz seems play a minor role in O^+ abundance at the dusk flank magnetopause during intense~~

387 ~~substrom. These results show~~Our result of O^+ density increase with IMF B_y also agree with Kronberg et

388 al., (2012). They showed for 10 keV O^+ strong increasing under the duskward IMF indicated by the clock

389 angle in the inner magnetosphere. It is suggested that the O^+ abundance at the ~~dusk flank~~duskside

390 magnetopause ~~have~~ has a corresponding relation with the O^+ in the duskside near-Earth ~~plasma~~

391 ~~sheet~~magnetosphere during intense substorm. The O^+ path from the cusp to the magnetotail is asymmetry

392 and it has the best correlation with the IMF directions. This path asymmetry mainly controlled by the

393 IMF B_y may influence on O^+ abundance at the duskside magnetopause. When the IMF B_y is positive, the

394 O^+ from northern/southern cusp tends to flow toward the dawnside/duskside. The transport path for

395 negative IMF B_y is more symmetric but shows some evidence for a reversed asymmetry when the

396 negative IMF B_y is large enough. While the IMF B_z has little influence on the asymmetry (Liao et al.,

397 2010).

398 Due to not enough events occurred under northward IMF were observed, the influence of IMF B_z

399 on the O^+ abundance (1-40 keV) during intense substorm is not clear. While in Luo et al. (2017) study

400 that not only the cases for the intense substorm were considered, they found the O^+ intensity (> ~274 keV)

401 was significantly higher under southward IMF than that under northward IMF especially at the duskside

402 magnetopause. Zeng et al. (2019) also showed that the duskside asymmetry of O^+ density (1-40 keV) in

403 the dayside magnetopause under northward IMF was less obvious than under southward IMF when the

404 IMF B_y was the same. Under the southward IMF, the interactions between the solar wind and the

405 magnetosphere become active. The inductive electric field or magnetic field gradient related to magnetic

406 reconfiguration will enhance with negative IMF B_z. So the large scale dawn-dusk electric field drift along

407 with the gradient-curvature drift can force oxygen ions convect to the duskside magnetopause boundary

408 layer (Kronberg et al., 2015; Luo et al., 2017).

409   In this statistical study, there are 50 magnetopause boundary layer crossing events during intense

410 substorm under southward IMF with respect to 7 events under northward IMF. Choosing the intense

411 substorm may increase the probability of observing the events under southward IMF quite significantly.

412 Among ~~our 31~~ 57 events of energetic O^+ near the ~~dusk flank~~duskside magnetopause, there are ~~9~~26 events

413 during intense substorm expansion phase which are all under the southward IMF, as the blue circle shown

414 in Figure 6b. ~~Hsu, T. - S., and McPherron, R. L. (2003) found that approximately 60% of all substorms~~

415 ~~expansion phase are correspond to the northward IMF Bz. But,t~~There are only ~~6~~7 events under ~~the~~

416 northward IMF in our study and they all occurred during the intense substorm recovery phase. But what

417 relation between the IMF directions and phase of substorm is out of scope for this article. ~~Thus our~~

418 ~~statistical results demonstrate that the energetic O^+ near the dusk flank magnetopause dominated~~

419 ~~occurring under the southward IMF.~~

420   Previous research~~es~~ demonstrated that the oxygen ions origin from the aurora region ~~can~~ could

421 rapidly feed in the ~~near-Earth plasma sheet~~NEPS ~~in the magnetotail~~ during intense substorms expansion

422 phase (e.g., Daglis and Axford, 1996; Duan et al, 2017; Yu et al., 2013). Oxygen ions can be efficiently

423 energized in the ~~near-Earth plasma sheet~~NEPS during intense substorm dipolarization (e.g., Duan et al.,

424 2017; Fok et al., 2006; Nos~~é~~e et al., 2000). Under southward IMF conditions, these energetic oxygen

425 ions in the NEPS can be convected sunward and drift westward. As a result, the energetic O^+ arrived near

426 the ~~dusk flank~~duskside magnetopause ~~during intense substorm expansion phase could~~ can participate in

427 the magnetopause reconnection and escape along reconnected field lines during intense substorm

428 expansion phase, as reported by Wang et al. (2014) and Zong et al. (2001). ~~But from Fuselise et al. (2019),~~

429 ~~while~~When O^+ participate in the reconnection jets, the reconnection rate ~~is~~will likely be reduced by the

430 mass-loading ~~, reconnection is~~but not suppressed at the magnetopause (Fuselier et al. 2019). Whether

431 these energetic O^+ at the duskside boundary layer could suppress the intense substorm need further

432 investigation.

5 Summary and conclusions

Using the measurements from ~~FPI, HPCA and FGM on~~ MMS ~~mission~~ satellite during the phase 1~~a~~ ~~and 1b~~, we have studied ~~31~~ 57 events of the energetic ~~oxygen ions~~O^+ (1-40 keV) ~~distributions~~ at the ~~dusk flank~~duskside magnetopause boundary layer and their variations on the solar wind conditions (IMF B_y, IMF B_z and solar wind dynamic pressure) during intense substorm expansion phases and recovery phases. According to the above analysis, we can draw our main conclusions as follows. ~~During intense substorms, the energetic oxygen ions are mainly observed at the dusk flank magnetopause within the substorm recovery phase.~~ In our ~~31~~ 57 events of energetic O^+ at the ~~dusk flank~~duskside magnetopause boundary layer, there are ~~only 9~~26 events during the expansion phase of intense substorms and 31 events during the recovery phase. ~~While there are 22 events during the recovery phase of intense substorms.~~ It is noted that the mean values of the O^+ density during the expansion phase and recovery phases are 0.069 cm^{-3} and 0.081 cm^{-3}, respectively. And the maximum O^+/H^+ density ratio occurred during the intense substorm recovery phase. ~~We find out~~It is found that ~~9~~26 events of energetic O^+ at the ~~dusk flank~~duskside magnetopause during intense substorms expansion phase are all under the southward IMF conditions, and only 7 events under northward IMF which are all during the intense substorm recovery phase. The O^+ density shows an exponential increase with IMF B_z absolute value under the southward IMF. Similarly, it also presents an exponential growth with solar wind dynamic pressure, and the empirical functional relations are established. Like previous studies during substorm in the near-Earth magnetosphere, The O^+/H^+ ~~number~~ density ratio in the duskside magnetopause boundary layer ~~exponential increase~~enhance with the IMF B_y ~~and the maximum number density ratio of oxygen ion to proton is ~ 0.055 during intense substorm recovery phase~~. It is suggested that the O^+ abundance in the duskside magnetopause boundary layer has a close correlation with the O^+ variations in the near-Earth magnetosphere during intense substorm. ~~The high energetic O^+ number density at the dusk flank magnetopause during intense substorms is in the range from 0.01 cm^{-3} to 0.2 cm^{-3}. Our observations suggest that energetic oxygen ions are a key indicator in the mass and energy transport from the tail to the dayside in the magnetosphere during intense substorms.~~

Data availability

All data used in this study are publicly accessible. MMS data are available at the MMS Science Data Center (https://lasp.colorado.edu/mms/sdc/public/). The OMNI data can be downloaded from the NASA Goddard Space Flight Center Coordinated Data Analysis Web (CDAWeb:http://cdaweb.gsfc.nasa.gov/).

Competing interests

The authors declare that they have no conflict of interest.

Author contribution

C. Z. conducted the majority of the data processing, analysis and writing for this study. S.P.D, C.W, L.D and S.F participated in the interpretation of the data and modified this paper. J.B, R.T, B.G and C.R produced the data and controlled the data quality. All the authors discussed the results and commented on the paper.

References

Angelopoulos, V., Cruce, P., Drozdov, A. et al. (2019), The Space Physics Environment Data Analysis System (SPEDAS), Space Sci Rev., 215(9), doi:10.1007/s11214-018-0576-4.

Birn, J., Thomsen, M. F., and Borovsky, J. E. et al.: Substorm ion injections: Geosynchronous observations and test particle orbits in three-dimensional dynamic MHD fields, J. Geophys. Res., 102, 2325–2341, 1997.

Bouhram, M., Klecker, B., Paschmann, G., Haaland, S., Hasegawa, H., Blagau, A., et al. (2005). Survey of energetic O^+ ions near the dayside mid-latitude magnetopause with Cluster. Annales Geophysicae, 23(4), 1281–1294. doi:10.5194/angeo-23-1281-2005.

486 Burch, J. L., Moore, T. E., Torbert, R. B., and Giles, B. L. (2016). Magnetospheric Multiscale
487   Overview and Science Objectives. Space Science Reviews, 199(1–4), 5–21.
488   doi:10.1007/s11214-015-0164-9.

489 Daglis, I. A., N. P. Paschalidis, E. T. Sarris, W. I. Axford, G. Kremser, B. Wilken, and G. Gloeckler
490   (1991), Statistical features of the substorm expansion phase as observed by AMPTE/CCE
491   spacecraft, in Magnetospheric Substorms, Geophys. Monogr. Ser, vol. 64, edited by J. R. Kan
492   et al., pp. 323–332, AGU, Washington, D. C.

493 Daglis, I. A., Livi, S., Sarris, E. T., and Wilken, B. (1994), Energy density of ionospheric and solar
494   wind origin ions in the near‐Earth magnetotail during substorms, J. Geophys.
495   Res., 99(A4), 5691–5703, doi:10.1029/93JA02772.

496 Daglis, I. A., ~~&~~ and Axford, W. I. (1996). Fast ionospheric response to enhanced activity in geospace:
497   Ion feeding of the inner magnetotail. Journal of Geophysical Research, 101(A3), 5047–5065,
498   doi:10.1029/95JA02592.

499 ~~Daglis, I. A., R. M. Thorne, W. Baumjohann, and S. Orsini (1999), The terrestrial ring current: Origin,~~
500   ~~formation, and decay, Rev. Geophys., 37, 407, doi:10.1029/1999RG900009.~~

501 Dai, L., J. R. Wygant, C. A. Cattell, S. Thaller, K. Kersten, A. Breneman, X. Tang, R. H. Friedel, S. G.
502   Claudepierre, and X. Tao (2014), Evidence for injection of relativistic electrons into the
503   Earth's outer radiation belt via intense substorm electric fields, Geophys. Res. Lett., 41, 1133–
504   1141,doi:10.1002/2014GL059228.

505 Dai, L., Wang, C., Duan, S., He, Z., Wygant, J. R., Cattell, C. A.,…Tang, X. (2015). Near-Earth
506   injection of MeV electrons associated with intense dipolarization electric fields: Van Allen
507   Probes observations. Geophysical Research Letters, 42, 6170–6179. https://doi.org/10.1002/
508   2015GL064955.

509 Duan, S. P., Liu, Z. X., Liang, J., Zhang, Y. C., ~~&~~ and Chen, T. (2011). Multiple magnetic
510   dipolarizations observed by THEMIS during a substorm. Annales de Geophysique, 29(2),
511   331–339, doi:10.5194/angeo- 29- 331- 2011.

512 Duan, S. P., L. Dai, C. Wang, J. Liang, A. T. Y. Lui, L. J. Chen, Z. H. He, Y. C. Zhang, and V.
513   Angelopoulos (2016), Evidence of kinetic Alfvén eigenmode in the near-Earth magnetotail
514   during substorm expansion phase, J. Geophys. Res. Space Physics, 121, 4316–4330,
515   doi:10.1002/ 2016JA022431.

516 Duan, S., Dai, L., Wang, C., He, Z., Cai, C., Zhang, Y. C., … Khotyaintsev, Y. V. (2017). Oxygen ions
517   O^+ energized by kinetic Alfvén eigenmode during dipolarizations of intense substorms.
518   Journal of Geophysical Research: Space Physics, 122. https://doi.org/10.1002/ 2017JA024418

519 Ebihara, Y., M.‐C. Fok, T. J. Immel, and P. C. Brandt (2011), Rapid decay of storm time ring current
520   due to pitch angle scattering in curved field line, J. Geophys. Res., 116, A03218,
521   doi:10.1029/2010JA016000.

522 Elliott, H. A., Comfort, R. H., Craven, P. D., Chandler, M. O., and Moore, T. E. (2001), Solar wind
523   influence on the oxygen content of ion outflow in the high‐altitude polar cap during solar
524   minimum conditions, J. Geophys. Res., 106(A4), 6067–6084, doi:10.1029/2000JA003022.

525   Ergun, R. E., Tucker, S., Westfall, J., Goodrich, K. A., Malaspina, D. M., Summers, D., et al. (2016).
526   The Axial Double Probe and Fields Signal Processing for the MMS Mission. Space Science
527   Reviews, 199(1–4), 167–188. doi:10.1007/s11214-014-0115-x.

528   Fok, M., Moore, T. E., Brandt, P. C., Delcourt, D. C., Slinker, S. P., ~~&~~ and Fedder, J. A. (2006).
529   Impulsive enhancements of oxygen ions during substorms. Journal of Geophysical Research,
530   111, A10222, doi:10.1029/2006JA011839.

531   ~~Frank, L. A., W. R. Paterson, and J. B. Sigwarth (2002), Observations of plasma injection into the ring~~
532   ~~current during substorm expansive phase, J. Geophys. Res., 107(A11), 1343,~~
533   ~~doi:10.1029/2001JA000169.~~

534   Fuselier, S. A., Klumpar, D. M., Peterson, W. K., and Shelley, E. G. (1989), Direct injection of
535   ionospheric O^+ into the dayside low latitude boundary layer. Geophysical Research Letters,
536   16(10), 1121–1124. doi.:10.1029/GL016i010p01121.

537   Fuselier, S. A., D. M. Klumpar, and E. G. Shelley (1991), Ion reflection and transmission during
538   reconnection at the Earth's subsolar magnetopause, Geophys. Res. Lett., 18, 139–142,
539   doi:10.1029/90GL02676.

540   Fuselier, S. A., et al. (2016a), Magnetospheric ion influence on magnetic reconnection at the duskside
541   magnetopause, Geophys. Res. Lett., 43,1435–1442, doi:10.1002/2015GL067358.

542   Fuselier, S. A., Lewis, W. S., Schiff, C., Ergun, R., Burch, J. L., Petrinec, S. M., and Trattner, K. J.
543   (2016b). Magnetospheric Multiscale Science Mission Profile and Operations. Space Science
544   Reviews, 199(1–4), 77–103. doi:10.1007/s11214-014-0087-x.

545   Fuselier, S. A., Trattner, K. J., Petrinec, S. M., Denton, M. H., Toledo‑Redondo, S., André, M., et al.
546   (2019).Mass loading the Earth's dayside magnetopause boundary layer and its effect on
547   magnetic reconnection. Geophysical Research Letters, 46, doi:10.1029/2019GL082384.

548   Ganushkina, N. Y., Pulkkinen, T. I., ~~&~~ and Fritz, T. (2005). Role of substorm-associated impulsive
549   electric fields in the ring current development during storms. Annales Geophysicae, 23(2),
550   579–591, doi:10.5194/angeo-23-579-2005.

551   ~~Hsu, T.‑S., and McPherron, R. L. (2003), Occurrence frequencies of IMF triggered and nontriggered~~
552   ~~substorms, J. Geophys. Res., 108, 1307, doi:10.1029/2002JA009442, A7.~~

553   Kim, K. C., Lee, D.‑Y., Lee, E. S., Choi, C. R., Kim, K. H., Moon, Y. J., Cho, K. S., Park, Y. D.,
554   and Han, W. Y. (-2005), A new perspective on the role of the solar wind dynamic pressure in
555   the ring current particle loss through the magnetopause, J. Geophys. Res., 110, A09223,
556   doi:10.1029/2005JA011097.

557   Kronberg, E. A., Haaland, S. E., Daly, P. W., Grigorenko, E. E., Kistler, L. M., Fränz, M., and
558   Dandouras, I. (2012), Oxygen and hydrogen ion abundance in the near-Earth magnetosphere:
559   Statistical results on the response to the geomagnetic and solar wind activity conditions, J.
560   Geophys. Res., 117, A12208, doi:10.1029/2012JA018071.

561   ~~Keika, K., P. C. Brandt, M. Nosé, and D. G. Mitchell (2011), Evolution of ring current ion energy~~
562   ~~spectra during the storm recovery phase: Implication for dominant ion loss processes, J.~~
563   ~~Geophys. Res., 116, A00J20, doi:10.1029/2010JA015628.~~

Keika, K., L. M. Kistler, and P. C. Brandt (2013), Energization of O+ ions in the Earth's inner magnetosphere and the effects on ring current buildup: A review of previous observations and possible mechanisms, J. Geophys. Res. Space Physics, 118, 4441–4464, doi:10.1002/jgra.50371.

Kronberg, E. A., Ashour-Abdalla, M., Dandouras, I., Delcourt, D. C., Grigorenko, E. E., Kistler, L. M.,…Zelenyi, L. M. (2014). Circulation of heavy ions and their dynamical effects in the magnetosphere: Recent observations and models. Space Science Reviews, 184(1-4), 173–235, doi:10.1007/s11214-014-0104-0.

Kronberg, E. A., E. E. Grigorenko, S. E. Haaland, P. W. Daly, D. C. Delcourt, H. Luo, L. M. Kistler, and I. Dandouras (2015), Distribution of energetic oxygen and hydrogen in the near-Earth plasma sheet, J. Geophys. Res. Space Physics, 120, 3415–3431, 681 doi:10.1002/2014JA020882.

Lennartsson, W., and Shelley, E. G. (1986). Survey of 0.1- to 16-keV/ e plasma sheet ion composition. Journal of Geophysical Research, 91(A3), 3061.

Li, X., M. Hudson, A. Chan, and I. Roth (1993), Loss of ring current O^+ ions due to interaction with Pc 5 waves, J. Geophys. Res., 98, 215–231, doi:10.1029/92JA01540.

Liao, J., Kistler, L. M., Mouikis, C. G., Klecker, B., Dandouras, I., and Zhang, J.-C. (2010), Statistical study of O^+ transport from the cusp to the lobes with Cluster CODIF data, J. Geophys. Res., 115, A00J15, doi:10.1029/2010JA015613.

Liu, Y. H., C. G. Mouikis, L. M. Kistler, S. Wang, V. Roytershteyn, and H. Karimabadi (2015),The heavy ion diffusion region in magnetic reconnection in the Earth's magnetotail, J.Geophys. Res., 120, 3535-3551, doi:10.1002/2015JA020982.

Lindqvist, P.-A., Olsson, G., Torbert, R. B., King, B., Granoff, M., Rau, D., et al. (2016). The Spin-Plane Double Probe Electric Field Instrument for MMS. Space Science Reviews, 199(1–4), 137–165. doi:10.1007/s11214-014-0116-9.

Lui, A. T. Y., Liou, K., Nosé, M., Ohtani, S., Williams, D. J., Mukai, T., et al. (1999). Near-Earth dipolarization: Evidence for a non-MHD process. Geophysical Research Letters, 26(19), 2905–2908. Doi:10.1029/1999GL003620.

Luo, H., E. A. Kronberg, K. Nykyri, K. J. Trattner, P. W. Daly, G. X. Chen, A. M. Du, and Y. S. Ge (2017), IMF dependence of energetic oxygen and hydrogen ion distributions in the near-Earth magnetosphere, J. Geophys. Res. Space Physics, 122, 5168–5180, doi:10.1002/2016JA023471.

Moore, T. E., Arnoldy, R. L., Feynman, J., and Hardy, D. A.: Propagating substorm injection fronts, J. Geophys. Res., 86, 6713–6726, 1981, doi:10.1029/JA091iA03p03061.

Nosé, M., Lui, A. T. Y., Ohtani, S., Mauk, B. H., McEntire, R. W., Williams, D. J.,…Yumoto, K. (2000). Acceleration of oxygen ions of ionospheric origin in the near-Earth magnetotail during substorms. Journal of Geophysical Research, 105(A4), 7669–7677, doi:10.1029/1999JA000318.

602 Ohtani, S., M. Nosé, S. P. Christon, and A. T. Y. Lui (2011), Energetic O^+ and H^+ ions in the plasma
603   sheet: Implications for the transport of ionospheric ions, J. Geophys. Res., 116, A10211,
604   doi:10.1029/2011JA016532.

605 Ono, Y., M. Nosée, S. P. Christon, and A. T. Y. Lui (2009), The role of magnetic field fluctuations in
606   nonadiabatic acceleration of ions during dipolarization, J. Geophys. Res., 114, A05209,
607   doi:10.1029/2008JA013918.

608 Phan, T. D., Dunlop, M. W., Paschmann, G. et al.: Cluster observations of continuous reconnection at
609   the magnetopause under steady interplanetary magnetic field conditions, Ann. Geophys., 22,
610   2355–2367, 2004,

611 Pollock, C., Moore, T., Jacques, A., Burch, J., Gliese, U., Saito, Y., et al. (2016). Fast Plasma
612   Investigation for Magnetospheric Multiscale. Space Science Reviews, 199(1–4), 331–406.
613   doi:10.1007/s11214-016-0245-4.

614 Russell, C. T., Anderson, B. J., Baumjohann, W., Bromund, K. R., Dearborn, D., Fischer, D., et al.
615   (2016). The Magnetospheric Multiscale Magnetometers. Space Science Reviews, 199(1–4),
616   189–256. doi:10.1007/s11214-014-0057-3.

617 Shue, J. ‑ H., et al. (1998), Magnetopause location under extreme solar wind conditions, J. Geophys.
618   Res.,103(A8), 17691– 17700, doi:10.1029/98JA01103.

619 Sonnerrup, B. U. Ö., G. Paschmann, I. Papamastorakis, N. Sckopke, G. Haerendel, S. J. Bame, J. R.
620   Asbridge, J. T. Gosling, and C. T. Russell (1981), Evidence for magnetic field reconnection at
621   the Earth's magnetopause, J. Geophys. Res., 86, 10,049–10,067,
622   doi:10.1029/JA086iA12p10049.

623 Slapak, R., H. Nilsson, L. G. Westerberg, and A. Eriksson (2012), Observations of oxygen ions in the
624   dayside magnetosheath associated with southward IMF, J. Geophys. Res., 117, A07218,
625   doi:10.1029/2012JA017754.

626 Slapak, R., Nilsson, H., Westerberg, L. G., and Larsson, R (2015), O^+ transport in the dayside
627   magnetosheath and its dependence on the IMF direction, Ann. Geophys., 33, 301-307,
628   doi:10.5194/angeo-33-301-2015.

629 Tang, B., and Wang, C. (2018). Large scale current systems developed from substorm onset: Global
630   MHD results. Science China Technological Sciences, 61(3), 389–396, doi:10.1007/s11431-
631   017-9132-y.

632 Wang, S., L. M. Kistler, C. G.Mouikis, Y. Liu, and K. J. Genestreti (2014), Hot magnetospheric O^+ and
633   cold ion behavior in magnetopause reconnection: Cluster observations, J. Geophys.Res., 119,
634   9601-9623, doi:10.1002/2014JA020402.

635 Welling, D. T., Jordanova, V. K., Zaharia, S. G., Glocer, A., and Toth, G. (2011), The effects of
636   dynamic ionospheric outflow on the ring current, J. Geophys. Res., 116, A00J19,
637   doi:10.1029/2010JA015642.

638 Winglee, R. M., Lewis, W., and Lu, G. (2005), Mapping of the heavy ion outflows as seen by IMAGE
639   and multifluid global modeling for the 17 April 2002 storm, J. Geophys. Res., 110, A12S24,
640   doi:10.1029/2004JA010909.

641 Winglee, R. M., and Harnett, E. (2011), Influence of heavy ionospheric ions on substorm onset, J.
642   Geophys. Res., 116, A11212, doi:10.1029/2011JA016447.

643 Yau, A. W., and M. André (1997), Sources of ion outflow in the high latitude ionosphere, Space Sci.
644   Rev., 80, 1.

645 Yau, A. W., A. Howarth, W. K. Peterson, and T. Abe (2012), Transport of thermal-energy ionospheric
646   oxygen (O^+) ions between the ionosphere and the plasma sheet and ring current at quiet times
647   preceding magnetic storms, J. Geophys. Res., 117, A07215, doi:10.1029/2012JA017803.

648 Yu, Y., and A. J. Ridley (2013), Exploring the influence of ionospheric O^+ outflow on magnetospheric
649   dynamics: dependence on the source location, J. Geophys. Res. Space Physics, 118, 1711–
650   1722, doi:10.1029/2012JA018411.

651 Young, D. T., Burch, J. L., Gomez, R. G., De Los Santos, A., Miller, G. P., Wilson, P., et al. (2016).
652   Hot Plasma Composition Analyzer for the Magnetospheric Multiscale Mission. Space Science
653   Reviews, 199(1–4), 407–470. doi:10.1007/s11214-014-0119-6.

654 Zeng, C., Duan, S., Wang, C., Dai, L., Fuselier, S., et al. (2019). Statistical study of oxygen ions
655   abundance and spatial distribution in the dayside magnetopause boundary layer: MMS
656   observations, J. Geophys. Res. Space Physics, under review.

657 Zong, Q. ‑ G., Wilken, B., Fu, S. Y., Fritz, T. A., Korth, A., Hasebe, N., Williams, D. J., and Pu, Z. ‑
658   Y. (2001),Ring current oxygen ions escaping into the magnetosheath, J. Geophys.
659   Res., 106(A11), 25541– 25556, doi:10.1029/2000JA000127.

660 **Figures and Captions**

661 **Figure 1.** The three components of the IMF B_x, B_y, B_z in the Geocentric Solar Magnetospheric
662 coordinates, solar wind dynamic pressure, as well as AU, AL and AE index from CDAweb OMNI data.
663 The two blue dashed lines indicate the interval of the magnetopause boundary layer crossing.

664 **Figure 2.** The energetic O^+ is observed at the magnetopause during an intense substorm on 03 October
665 2015 by MMS 4. From top to bottom are (a) the magnetic field three components, Bx (blue line), By
666 (gree line), Bz (red line) and the total magnitude Bt (black line), (b) the electric field three components,
667 Ex (blue), Ey (gree) and Ez (red), (c) ion parallel (red) and perpendicular (black) temperatures, as well
668 as electron parallel (blue) and perpendicular (green) temperatures, (d) The density of ion (green) and
669 electron (blue), (e) three components of the ion velocity, (f) the H^+ (over the full HPCA energy range
670 from 1 eV to 40 keV) and O^+ (at energies from 1 keV to 40 keV) densities, (g-h) electron and ion
671 omnidirectional differential energy fluxes (keV/(cm^2 s sr KeV)$^{-1}$), (i) to (l) present differential particle
672 fluxes (cm^2 s sr eV)$^{-1}$ of H^+, O^+, He^+, He^{++}, respectively. The Geocentric Solar Magnetospheric coordinate
673 system is adopted. The thick bars at the top of the panel present different regions encountered on this
674 magnetopause crossing event. The orange and blue bars represent the magnetosheath and the
675 magnetosphere, respectively. The green bar represents the magnetopause boundary layer. The black

horizontal line in figure 2j is at 1 keV and the O⁺ contamination from high H⁺ fluxes is indicated by the red box. The FPI data in Figure 2c-e and g-h are from FPI L2 data products and in the fast mode.

Figure 3. Maps of 31 events of energetic O⁺ at the ~~dusk flank~~duskside magnetopause during intense substorms with AE index larger than 500 nT in XY$_{GSM}$ plane. The O+ ~~number~~density and the ~~number~~ density ratio~~s~~ of O⁺/H⁺ are shown by the color signatures at the corresponding magnetopause location in Figure~~s~~ 3a and 3b, respectively. The blue curve line represents the nominal magnetopause. The diamond and circle represent the event at the magnetopause during the intense substorm expansion phase and recovery phase, respectively.

Figure 4. The relationship between the energetic O⁺ at the ~~dusk flank~~duskside magnetopause and AE index during intense substorms. From top to bottom, panels show ~~that~~ the O⁺ and H⁺ ~~number~~density~~ies,~~ (Figure 4a), the O⁺/H⁺ ~~number~~density ratio~~of O⁺/H⁺,~~ (Figure 4b), and O⁺/H⁺ particle flux ratio~~n of O+/H+,~~ (Figure 4c), respectively. Error bars indicate ~~95~~90% confidence intervals.

Figure 5. The relationship between the energetic O⁺ at the ~~dusk flank~~duskside magnetopause and IMF B$_y$ during intense substorms. The format is the same as that of Figure 4.~~From top to bottom, panels show that the O+ and H+ number density, Figure 7a, the number density ratio of O+/H+, Figure 7b, and particle flux ration of O+/H+ Figure 7c, respectively. Error bars indicate 95% confidence intervals.~~

Figure 6. The relationship between the energetic O+ at the ~~dusk flank~~duskside magnetopause and IMF B$_z$ during intense substorms. The format is the same as that of Figure 4. ~~From top to bottom, panels show that the O+ and H+ number density, Figure 7a, the number density ratio of O+/H+, Figure 7b, and particle flux ration of O+/H+ Figure 7c, respectively. Error bars indicate 95% confidence intervals.~~

Figure 7. The relationship between the energetic O+ at the ~~dusk flank~~duskside magnetopause and solar wind dynamic pressure during intense substorms. The format is the same as that of Figure 4.~~From top to bottom, panels show that the O+ and H+ number density, Figure 7a, the number density ratio of O+/H+, Figure 7b, and particle flux ration of O+/H+ Figure 7c, respectively. Error bars indicate 95% confidence intervals.~~